MASTER'S THESIS

Parameter identification and simulation of conducting polymer micro-sensors using global spectral projection methods

by Ashish Sabadra
Advisor: Raymond A. Adomaitis, Thomas J. McAvoy

MS 2001-1

ABSTRACT

Title of Thesis:	Parameter Identification and Simulation
	of Conducting Polymer Micro-Sensors
	using Global Spectral Projection Methods
Degree candidate:	Ashish Sabadra
Degree and year:	Master of Science, 2001
Thesis directed by:	Assistant Professor Raymond A. Adomaitis
	Department of Chemical Engineering
	Institute for System Research

Chemical micro-sensors have the potential of a wide range of applications that include odor sensing in food industry, environmental monitoring, improved process control, detection of hazardous chemicals, medical diagnosis, and control of automobile emissions. In this thesis, a model is developed describing the electrical response of a thin-film, conducting polymer sensor to an air mixture containing different target gas species. Numerical methods for discretizing the initial-boundary value problem defining the film conductance model are presented. Nonlinear parameter identification methods are used to identify a subset of the model parameters.

Two models of sensor operation are studied. In the first case, the isothermal response of the sensor to time varying gas phase concentration is considered. The

effectiveness of sensor cleaning is studied in the second case in which the sensor substrate temperature is periodically increased to drive out adsorbed gas species. Good agreement is found when model predictions are compared with published experimental results.

Parameter Identification and Simulation

of Conducting Polymer Micro-Sensors

using Global Spectral Projection Methods

by

Ashish Sabadra

Thesis submitted to the Faculty of the Graduate School of the
University of Maryland at College Park in partial fulfillment
of the requirements for the degree of
Master of Science
2001

Advisory Committee:

Assistant Professor Raymond A. Adomaitis, Chairman/Advisor
Professor Thomas McAvoy
Associate Professor Michael Harris
Assistant Professor Sheryl Ehrman

TABLE OF CONTENTS

LIST OF TABLES

LIST OF FIGURES

Chapter 1

Introduction

1.1   Micro-sensors

Classical techniques such as Gas chromatography, ion mobility spectroscopy and mass spectroscopy are used for sensing purposes. These have been replaced in some applications by chemically sensitive solid state devices and conducting polymer based chemical micro-sensors. Micro-sensors are widely used for sensing odor, monitoring and control of chemical processes, detection of hazardous chemicals, and control of automobile emission. The thesis focuses on the chemical microsensor whose electrical properties are affected by the presence of certain gas species. There are other types of solid state chemical sensor based on acoustics (Bulk and surface acoustic waves (BAW and SAW)), optics (Optical waveguide) and thermochemistry (microcalorie sensor and microenthalpy sensor).

Some of the essential or desirable properties of the chemical micro-sensors are summarized as follows.

1. *Selectivity*

    The chemical sensor must respond to a range of chemical species to be

detected. The sensors should not have broadly overlapping sensitivities to discriminate between different chemicals.

2. *Sensitivity*

The chemicals to be detected may be present in the concentration range of ppm. The sensor should be sufficiently sensitive to detect small concentration level of gaseous species.

3. *Speed of response*

In order to be used for online measurements, the response time of the sensor should be in the range of seconds.

4. *Reproducibity*

The individual sensor element should be reproducible in their manufacture and response characteristics. This will reduce the task of calibrating each sensor element before use. Fabrication processes used to make a single sensor must be compatible with the manufacture of an array of reasonable size. Additionally, the sensors should have an inherently linear response characteristic.

5. *Reversibility*

The sensor should be able to recover after exposure to gas. If the process of absorption of gas in the polymer film is completely reversible, the sensor will not degrade and the response will not drift in the subsequent cycles.

6. *Portability*

Devices should be small so that small sample volumes can be used. The power consumption should be low so that the device can be operated with a battery, making the sensor portable [24].

1.2 Conducting polymer micro-sensors

Physical and electrical properties of conducting polymers are altered significantly by a selective interaction with some chemical species. Hence, conducting polymer films have been widely used in thin-film gas sensors, such as those found in commercially available "artificial noses" [18]. Conducting polymer gas sensors have a number of properties that make them attractive for commercial use. Sensors can be fabricated easily by electro-polymerization in a controlled manner using a wide range of basic monomers. Different chemicals can be added during the process of polymerization. The monomers react with these chemicals during the process of polymerization to give a wide range of polymer material. Additionally, different electrolytes and solvents during the process of electro-polymerization give rise to polymers with different properties. Large numbers of chemically distinct polymer provide an almost limitless number of chemically distinct polymers. Different polymers show non-overlapping selectivity towards different chemicals, hence an array of polymer sensors can be used to generate a pattern of response to distinguish different gas species. Polymer films respond reasonably rapidly and reversibly at room temperature to some chemicals. Thus, the advantages of the conducting polymer based sensors are reversibility, use at room temperature, low power consumption, and sensitivity to polar molecules [18].

1.3 Deposition techniques

The deposition technique and conditions during the process of deposition of polymer film on the substrate influence the electrical properties of the conducting polymer, hence a discussion of the deposition techniques is included in this the-

sis. Electro-polymerization and Langmuir Blodgett are the most commonly used techniques for the deposition of conducting polymer films; each method is discussed in the following sections.

1.3.1 Electro-polymerization technique

During the polymerization of pyrrole to form polypyrrole, pyrrole is oxidized to form a cation. The cation reacts with a neutral monomer to form a radical cation dimer. This propagation reaction continues the chain forming process. When the molecular weight of polypyrrole increases, its solubility decreases, finally precipitating to form nucleation sites. Due to the positive charge of the radical cation dimer of the oligomer, the precipitation occurs on the electrode surface. The nuclei grow by coupling between radical cation dimer of the precipitate oligomer and monomer in the solution.

The electro-polymerization technique is attractive and effective because the thickness of the coating can be controlled. The technique offers new possibilities for the design of coating which are reproducible in thickness and permeability. It also enables the synthesis of unusual polymers, which have not been obtained by any other methods [29].

1.3.2 Langmuir Blodgett technique

In the Langmuir Blodgett (LB) deposition technique, a solution of stearic acid in chloroform is spread onto a sub-phase of de-ionized water containing ferric chloride. The film is compressed and allowed to dry. After drying, the film is exposed to hydrochloric acid for a few minutes and then kept over pyrrole vapors for 24 hours [32].

The LB technique enables the formation of ultra-thin film structures. The thickness of the film can be controlled by altering the concentration of pyrrole vapors. The molecular arrangement in the polymer film is regular and uniform [15]. LB technique can be used to prepare an ordered monomolecular films and multi-layered structures with the required number of layers. LB film response to ethanol vapor is fast compared to electro-chemically deposited polypyrrole film. The quick response is probably due to high ratio of surface area to bulk volume in the LB film [32].

1.4 Objective of this thesis

Selectivity and sensitivity of the conducting layer and the transduction mechanism by which the chemical interaction is transformed into a measurable electrical signal are the two most important considerations in the design of a conductometric chemical sensor. The scope of this thesis is restricted to the discussion, simulation, and analysis of polymer film as the conducting layer.

The mechanisms accounting for the changes in electrical properties of conducting polymer films have been attributed to a wide range of phenomena [18]. It has been proposed that molecules bind to the polymer backbone forming a charge-transfer complex, changing the conductivity of the film. Therefore, a model describing the sensor response to gas concentration variations is described in terms of diffusion of the analyte species through the film layer and adsorption to vacant sites on the polymer backbone. Finally the relationship between the resulting site vacancy spatio-temporal distribution and the material conductance using a semi-infinite electrode geometry is computed to obtain the time-dependent electrical response. These modeling equations consist of time-dependent, nonlinear

boundary-value problems for each gas species. Models of this form are readily solved using global spectral methods software [2], recently expanded to include the data structures and methods that make possible an object-oriented approach to implementing the spectral projection methods [23]. The diffusion rate of gaseous species in the polymer, rate of adsorption and desorption of the gaseous species on the vacant sites and gas sensitivity coefficient of the polymer are estimated using the *MATLAB* optimization toolbox.

The simulated results are compared with the experimental values over a sequence of six adsorption and desorption cycles for the oxidizing and reducing gas species measured by Kendrick and co-workers [27]. Drift in the base resistance and decrease in sensitivity of the sensor in the context of the proposed model are discussed.

Rapid desorption of the gas from the polymer film at elevated temperature enables maximum reproducible sensitivity and baseline recovery. A new generation of conducting polymer gas sensor, namely, the *conductometric microhotplate gas sensor* [28][37] has been developed by researchers at National Institute of Standards and Technology (NIST) enabling operation of the sensor at elevated temperature. The temperature response of the film to variations in substrate temperature and temperature dependence of the forward/reverse sorption kinetics is modeled to simulate the time dependent electrical output of the conductometric microhotplate gas sensor.

Chapter 2

Computational tools

2.1 Previous work

Different computational tools have been employed for modeling response of chemical gas sensors. The finite element method and the electrical model method for modeling response of chemical gas sensors are discussed in the following sections.

2.1.1 Finite difference method

Gardner and co-workers have used the finite difference method to simulate the diffusion and adsorption of gas in the polymer film [18]. The explicit point method [12] was used with linear point spacing. Diffusion of gas through the polymer film was modeled by the finite difference form of the Fick's second law. The concentration of the gas at the inner boundary was determined by the five-point flux approximation method. Large number of iterations (of the order of one million or more) were required to achieve equilibrium for slow reactions, hence the finite difference method had the disadvantage of large computational time and accumulation of significant round-off errors for slow reactions. Crank-Nicholson

method was used to model diffusion in slow reactions. In [12] it was shown that Crank-Nicholson method reduced the simulation time by a factor of 100 for slow reactions. However, Crank-Nicholson method has a disadvantage that it can be applied to reaction kinetics of higher order than one only if simplifying approximations are used.

2.1.2 Electrical model method

The concept of an electrical equivalent circuit has also been used to solve the nonlinear partial differential equation describing the diffusion process in polymer film [9] [10]. In this approach, gas concentration and fractional occupancy are replaced with electrical voltages $u_{r,n}$ and $u_{\theta,n}$ respectively, as shown in figure (2.1). The gas concentration input is modeled by voltage source. The polymer film conductance is calculated by integrating $N + 1$ parallel current sources controlled by voltages $u_{\theta,n}$.
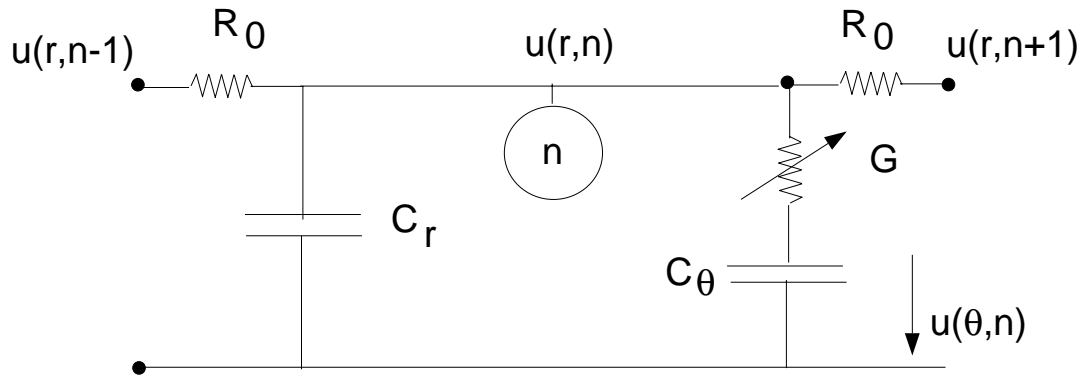
Figure 2.1: Electrical equivalent circuit for gas diffusion process and polymer film's conductance.

2.2   Spectral methods

The advantages of the Spectral methods over finite difference and finite element methods for numerical solution of partial differential equation models are discussed in *Numerical analysis of spectral methods* [20]. The advantages of spectral methods are summarized below.

The spectral method solution of a differential equation is expressed in terms of a truncated series of functions of the independent variables, hence the errors in the spectral method go to zero faster than any finite power of the number of retained modes. The finite difference and finite element methods yield finite order rates of convergence. Spectral methods require a factor of 2-5 fewer degrees of freedom in each space direction, resulting in considerable savings in terms of computational time. Additionally, the boundary conditions imposed on the spectral approximations are normally the same as those imposed on the differential equation [20].

2.3   MWR Tools

Methods for weighted residual (MWR) based on global spectral methods are a class of numerical techniques that include eigenfunction expansion, collocation, Galerkin and other projection methods [1][2][23][30]. They are used in the numerical solution and analysis of process systems described by partial differential equation models. The MWRtools library is a computational toolbox for implementing the MWR techniques in the *MATLAB* environment. It consists of *MATLAB* routines, which have one-to-one correspondence with each step of implementing a weighted residual method.

MWR solution to partial differential equations is formulated in terms of global functions. Number of functions is less than the number of discretization points. Hence non-polynomial functions, which satisfy the boundary conditions can be used. The functions can be accurately discretized and operations like integration and differentiation can be performed. Hence exact discrete analogs of the Galerkin technique and other MWR methods are reduced to matrix operations. The truncation error due to substitution of truncated series can be estimated and in some cases can also be exactly evaluated.

2.4   Spectral methods example

The temperature profile in a cylinder is modeled using spectral method to illustrate the application of spectral method for solving the boundary value problem.

Consider a long cylinder with a unit heat source. At steady state, the temperature profile along the radial direction is modeled in equation (2.1).

$$\nabla^2 T + 1 = 0 \tag{2.1}$$

The boundary conditions are given by equations (2.2) and (2.3).

$$\left.\frac{\partial T}{\partial r}\right|_{r=0} = 0 \tag{2.2}$$

$$T|_{r=1} = 0 \tag{2.3}$$

The physical domain is discretized using the *pd* routine. The problem geometry (*disk*) and number of discretization points (*npoints*) are parameters for the *pd* routine [2][30].

$$[r, wr, dr, ddr] = pd('disk', npoints)$$

Temperature is expressed in terms of trial function expansion (ψ).

$$T(t, r) = \sum_{i=1}^{N} a_i(t)\psi_i(r) \tag{2.4}$$

The trial functions are eigenfunctions of the Sturm-Liouville equation (equation 2.5).

$$\nabla^2\psi = \lambda\psi \tag{2.5}$$

The boundary conditions for the trial function are given by equations (2.6) and (2.7).

$$\psi|_{r=1} = 0 \tag{2.6}$$

$$\left.\frac{\partial\psi}{\partial r}\right|_{r=0} = 0 \tag{2.7}$$

The eigenfunctions are calculated using collocation based Sturm-Liouville problem solver (sl) [1].

$$[\Lambda, \psi] = sl('disk', dr, r, 1, 0, 0, 1, wr)$$

The truncated trial function expansion of temperature (equation 2.4) is substituted in the temperature profile (equation 2.1). The result projected onto each orthonormal trial function ψ_j gives the mode amplitude coefficients (a_j) at steady state (equation 2.8).

$$a_j = \frac{< -1, \psi_j >_{wr}}{\lambda_j} \tag{2.8}$$

The temperature profile is computed using the overloaded multiplication operator of *tfun* class [23]. The temperature profile in figure (2.2) is computed using 5, 10 and 20 discretization points and 1,2 and 5 trial functions respectively. The solution converges for five trial functions.
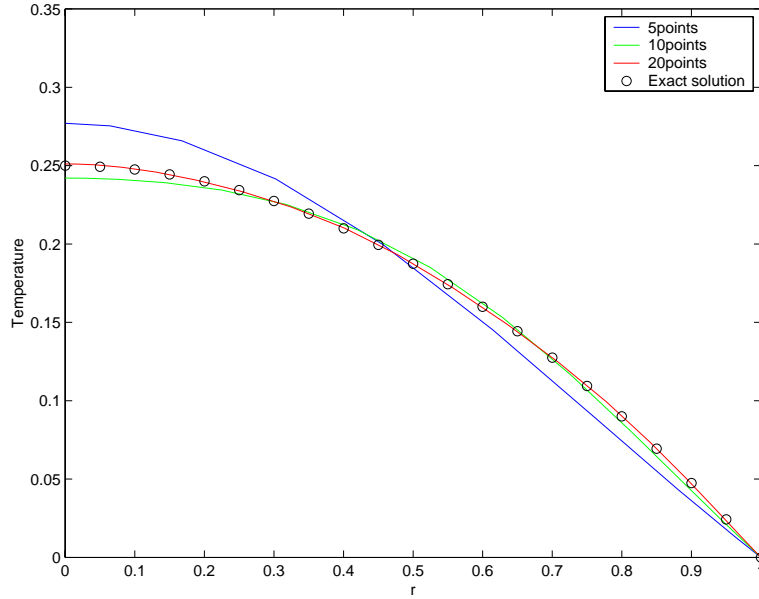
Figure 2.2: Temperature profile in a long cylinder along the radial direction

2.5 Parameter estimation and optimization

One objective of this thesis is to use parameter identification methods to produce accurate sensor models. Data from NIST researchers [27] will be used to determine the rate of diffusion (D), rate of adsorption (k_f) and desorption reaction (k_b) of the gaseous species and gas sensitivity coefficient of the polymer (S). The temperature dependency of these parameters is also identified.

Parameter estimation is an optimization problem because the solution is to minimize an objective function defined by the sum of the squares of the difference between the experimental data and model predictions. The rate of diffusion (D), rate of adsorption (k_f) and desorption reaction (k_b) should be greater than zero. We never ran into negative values for the above parameters during optimization, hence the parameters are considered unconstrained. The modeling equations are non-linear, hence parameter estimation leads to solving an unconstrained nonlin-

ear least square problem. The *lsqnonlin* function of the *MATLAB* optimization toolbox is used for parameter estimation. More details on the implementation of the parameter estimation will be provided later in this thesis.

Chapter 3

Isothermal sensors

3.1 Conductance Response Mechanisms

3.1.1 Charge transport

Polymers of a number of unsaturated organic chemicals display physico-chemical characteristics that cause them to behave as semiconductors. These polymers are obtained in their conducting form by formation of charge transfer complexes, as (P^+X^-) where P^+ denotes the polymer chain and X^- are anions like chlorates etc. These anions are called dopants [6]. The concentration of anions determines the doping level. Solid inorganic semiconductors have a maximum doping level of 6%. The doping level in conducting polymers is approximately 30%. Due to the high doping level, conducting polymers often exhibit metallic properties.

In polypyrrole, oxidation of the polymer breaks a double bond. A positive charge and a radical is formed on the polymer chain, called a *polaron* (figure 3.1). Polarons do not contribute significantly to the conductivity. The radical-cation (polaron) spreads out through adjacent π structure across the bond lengths to make contact with other radical-cation. Combination of two radicals, one
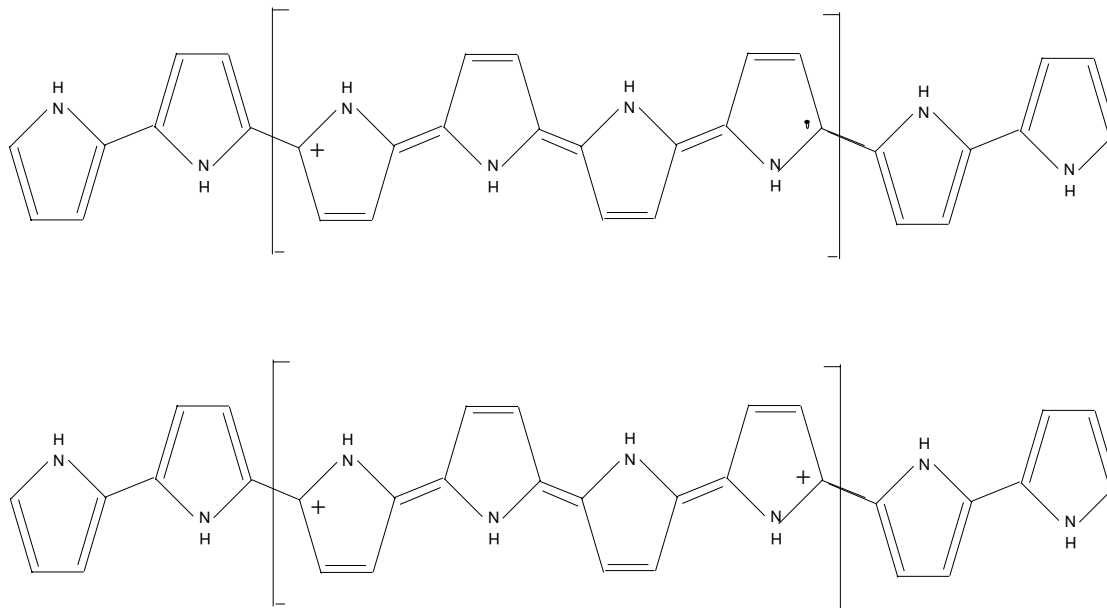
Figure 3.1: Polaron (top) and Bipolaron (bottom) in polypyrrole.

from each polaron, results in the formation of new π bond. This π bond is more stable than the two radical-cation pair. The result is a bipolaron, which is more stable than two polarons placed apart at the same distance. At low oxidation levels, the coulombic repulsion of positively charged polarons prevents the radicals from combining to form a bipolaron. When the extent of oxidation of the polymer increases, the concentration of polaron increases. They get close enough to combine and form a bipolaron [35].

In polypyrrole films with relatively low conductivity, electrons hopping between polaron and bipolaron defects govern the charge transport. The degree of disorder (cross-linking and branching) is fairly high, hence there is not much distinction between inter-chain and intra-chain hopping. The electron transport can be modeled by Mott's variable range hopping model (VRH) [42]. This model assumes thermally activated hopping by electrons with energies near the fermi

level. In high conducting polypyrrole films, mobility of the bipolaron along the chain plays an important part and contributes directly to the total conduction.

3.1.2 Band Structure

Oxidation of the polymer film gives rise to a new energy state. Removal of one electron from the π bond leaves the remaining electron in a non-binding orbital differing in energy from the valence and conduction states. These states are above the valence band and are responsible for the behavior of the polymer as though it was a heavily doped semi-conductor [35].

In the case of undoped polypyrrole chain, the gap between the valence band (VB) and the conduction band (CB) is 4.0 eV (figure 3.2a). At low doping levels (figure 3.2b), polarons are preferably formed. At an intermediate doping level (figure 3.2c), the polarons combine to give bipolarons. The bipolaron states overlap as the doping level increases. This process leads to the formation of bipolaron bands in the gap located 0.45 eV above the valence band edge and 0.9 eV below the conduction band edge. These bands have a width of 0.25 eV. At high doping level (100% doping), VEH calculations show that the bipolaron bands merges with the VB and CB (figure 3.2d). The original band gap of 4.0 eV is reduced to 1.4 eV.

3.1.3 Conductance mechanism

Absorption of gaseous species into the polymer film changes the conductivity of the sensor. The degree of change depends on the polymer film's affinity for the chemical and concentration of the gas species. The exact mechanism governing the film conductance response to gas composition is poorly understood. Five

16
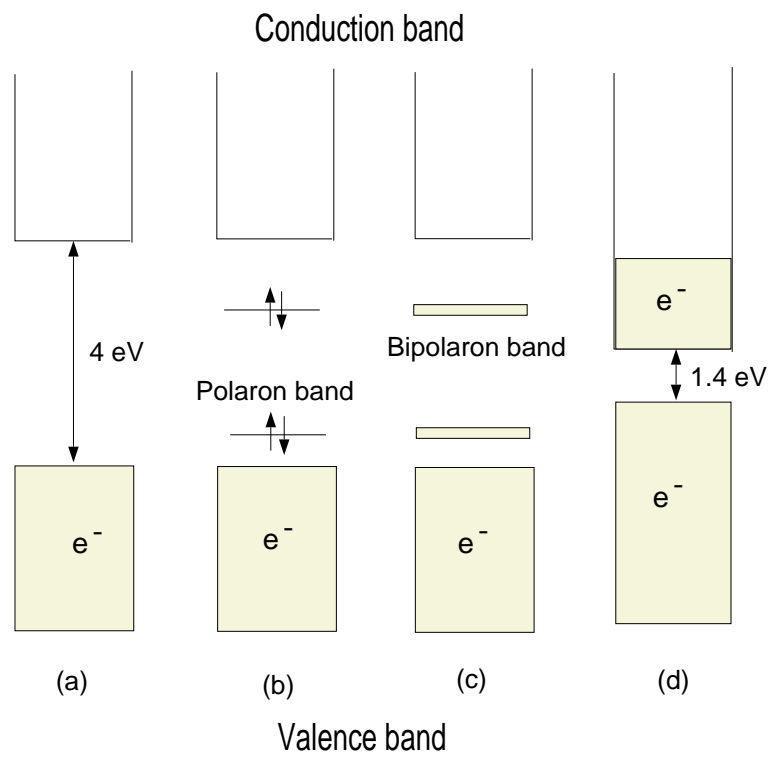
Figure 3.2: Band structure evolution upon doping of polypyrrole.

different mechanisms have been identified which might contribute to the overall observed gas sensitivity of the sensor [18]:

1. There can be direct generation or removal of charge carriers within the film due to the oxidation or reduction of the polymer by the gas.

2. Gas molecules can interact with the polymer chains leading to change in the mobility of the charge carriers.

3. The interaction of the counter-ion and vapor can change the polymer structure. This can affect the conductivity of the polymer film.

4. The adsorbed vapor can alter the intra-chain charge transfer process.

5. Gas molecules can affect the rate of interfacial charge transfer between the metal contact and the polymer film.

Although the exact mechanism of conductance in the polymer film is not known, the change in conductance for some chemicals can be predicted qualitatively. In the case of volatile organic compounds namely methanol, a charge transfer between the methanol molecules and polypyrrole produces a charge-transfer complex [11]. There are plasticization effects at high concentrations of methanol vapor [38]. The swelling of the polymer by methanol is the dominant effect. The polymer changes from a glass-like to a rubber-like state which affects its conducting behavior [36].

Polypyrrole behaves like a quasi 'p' type material. Resistance of the doped polypyrrole films increases in the presence of reducing gases. The electron donor gases donate electrons and remove the positive charge from the polymer backbone. The positive charge in the bipolaron is responsible for charge transfer in the polymers. The concentration of bipolaron decreases, resulting in a decrease in the conductivity of the polymer film. The reverse effect is observed in the case

of electron acceptor gases, which increase the positive charge leading to a greater concentration of the bipolaron and increased conductivity [25].

3.2   Modeling

A model is developed to simulate the response of a thin-film sensor, based on a design of NIST researchers [27], to a time varying gas composition. This model is similar in form to the model developed by Gardener and co-workers [16].

The conductance of polymer films is described by relatively simple functions of adsorption site occupancy on the conducting polymer backbone. The site vacancy is related to the gas phase composition through partial differential equation-based models of the species diffusion through the polymer film, coupled with sorption kinetics expressions.
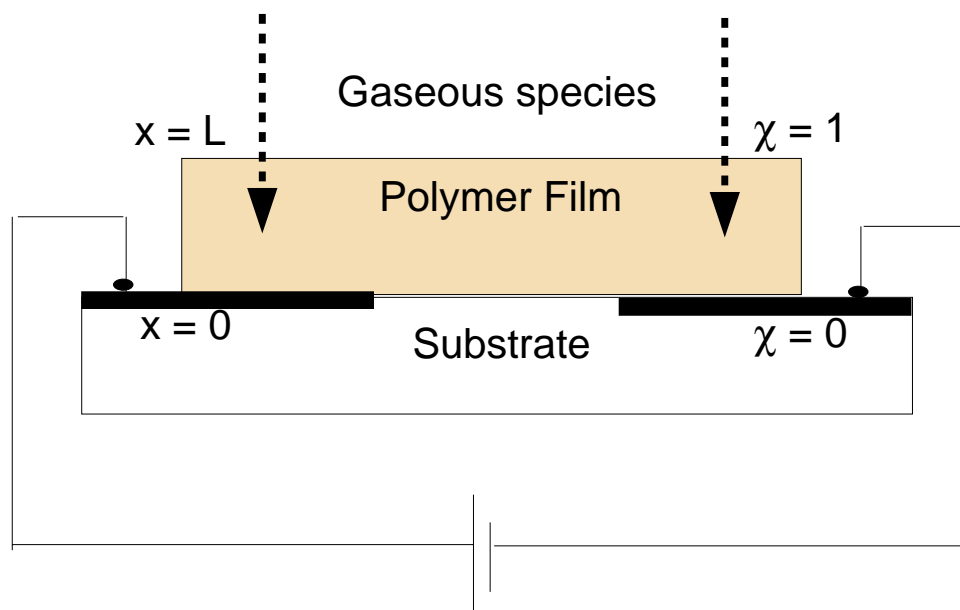
Figure 3.3: Schematic diagram of a conducting polymer film micro sensor.

The schematic diagram of a conducting polymer film micro-sensor is given in figure (3.3). Gaseous species A diffuses through the homogeneous polymer film of thickness L. The adsorption/desorption process is modeled by Langmuir adsorption isotherm (equation 3.1).

$$A + < Site > \rightleftharpoons \ < A > \tag{3.1}$$

We assume homogeneous distribution of the adsorption sites in the polymer. Since the thickness of the polymer film is small relative to the other dimensions, the geometry of the planar film is simplified to a one-dimensional model. Therefore, the sorbate concentration (C) and site occupancy (θ) profiles are only functions of distance (x) and time (t). The overall process can be expressed as rate of diffusion (equation 3.2) and rate of change of fractional site occupancy (equation 3.3).

$$\frac{\partial C}{\partial t} \ = \ D\frac{\partial^2 C}{\partial x^2} - N\frac{\partial \theta}{\partial t} \tag{3.2}$$

$$\frac{\partial \theta}{\partial t} \ = \ k_f C(1 - \theta) - k_b \theta \tag{3.3}$$

where k_f and k_b are rate of forward and backward adsorption kinetics. Since gas cannot diffuse through the substrate, the diffusive flux is equal to zero at the polymer film/substrate boundary $(x = 0)$.

$$\left.\frac{\partial C}{\partial x}\right|_{x=0} \ = \ 0 \tag{3.4}$$

The time varying gas concentration is described by a sequence of pulses of the target species in air. We assume that the concentration of the gaseous species in the polymer film surface exposed to the environment $(x = L)$ is equal to the species concentration in the environment (C_{ref}). The concentration of the gas species at the polymer film/gas interface is given as by equation (3.5).

$$C|_{x=L} \ = \ C_{ref}h(t) \tag{3.5}$$

where h is a square wave of unit amplitude. h is unity during adsorption and zero during desorption.

It is assumed that no gas is present in the polymer film initially. The initial condition for concentration is given by equation (3.6).

$$C|_{t=0} \ = \ 0 \tag{3.6}$$

The initial concentration for the subsequent desorption cycle is the amount of gas present in the conducting polymer due to adsorption (equation 3.7). Similarly, the gas remaining after desorption serves as the initial condition for adsorption cycle (equation 3.8).

$$C_{desorption} \ = \ C_{adsorption} \quad \forall \quad t = t_{cycle}(2n) \tag{3.7}$$

$$C_{adsorption} \ = \ C_{desorption} \quad \forall \quad t = t_{cycle}(2n-1) \tag{3.8}$$

where n ranges from one to the total number of adsorption/desorption cycles.

The dimensionless concentration (γ), time (τ) and length (χ) are defined by equation (3.9), (3.10) and (3.11) respectively.

$$\gamma \ = \ \frac{C}{C_{ref}} \tag{3.9}$$

$$\tau \ = \ \frac{t}{\frac{t_{cycle}}{2}} \tag{3.10}$$

$$\chi \ = \ \frac{x}{L} \tag{3.11}$$

where L is the thickness of the polymer film and t_{cycle} is the time of the adsorption/desorption cycle. Substituting the dimensionless quantities into the rate expression, boundary conditions, and initial conditions gives

$$\frac{\partial \gamma}{\partial \tau} \ = \ \frac{Dt_{cycle}}{L^2} \frac{\partial^2 \gamma}{\partial \chi^2} - \frac{N}{C_{Ref}} \frac{\partial \theta}{\partial \tau} \tag{3.12}$$

$$\frac{\partial \theta}{\partial \tau} \ = \ t_{cycle}(k_f C_{Ref} \gamma (1-\theta) - k_b \theta) \tag{3.13}$$

$$\left.\frac{\partial \gamma}{\partial \chi}\right|_{\chi=0} = 0 \tag{3.14}$$

$$\gamma|_{\chi=1} = \gamma_{bc}(\tau) \tag{3.15}$$

$$\gamma_{\tau=0} = 0 \tag{3.16}$$

$$\gamma_{adsorption} = \gamma_{desorption} \quad \forall \quad \tau = 2n - 1 \tag{3.17}$$

$$\gamma_{desorption} = \gamma_{adsorption} \quad \forall \quad \tau = 2n \tag{3.18}$$

The dimensionless parameters defining the diffusion coefficient of the gas species in the conducting polymer D', rate of adsorption K_f, and adsorption sites per unit concentration n_0 are given by equations (3.19), (3.20) and (3.21) respectively.

$$D' = \frac{D t_{cycle}}{L^2} \tag{3.19}$$

$$K_f = k_f C_{ref} \tag{3.20}$$

$$n_0 = \frac{N}{C_{ref}} \tag{3.21}$$

Substituting equation (3.13) in (3.12) and using the dimensionless quantities D', K_f, and n_0 gives equation (3.22).

$$\frac{\partial \gamma}{\partial \tau} = D'\frac{\partial^2 \gamma}{\partial \chi^2} - n_0 t_{cycle}(K_f \gamma(1 - \theta) - k_b \theta) \tag{3.22}$$

3.3   Numerical Solution

Object-oriented computational methods for implementing spectral projection techniques are used for solving the partial differential equations numerically. MWR tools package, developed specifically for solving boundary value problems by quadrature-based spectral projection methods [1][2][23][30], is used to solve the two differential equations (3.12) and (3.13).

The *pd* routine of *MWR tools* is used to set up the problem in terms of discrete points χ. The pd routine also defines the differentiation operator ∇^2. The

22

discretized physical domain, differentiation and quadrature array are defined for 40 points and *slab* geometry. The discretization point location and quadrature weights are based on the modified Gaussian quadrature method. The differentiation and Laplacian operators are based on Lagrange interpolation polynomial.

The boundary condition for concentration at the surface exposed to air ($x = L$) is not homogeneous. Hence the dimensionless concentration is split into components, which satisfy homogeneous boundary condition (γ_ω) and time-dependent non-homogeneous boundary condition ($\gamma_{\partial\omega}$) as shown in equations (3.23) and (3.24).

$$\gamma \;=\; \gamma_\omega + \gamma_{\partial\omega} \tag{3.23}$$

$$\;=\; \gamma_\omega + h(\tau)\chi^2 \tag{3.24}$$

In the Galerkin discretization procedure, the solution is represented in terms of an orthogonal function expansion where each trial function satisfies the boundary condition. The dimensionless concentration γ_ω and fractional site occupancy θ is expressed in terms of the trial functions ψ (equation 3.25) and ϕ (equation 3.26) respectively.

$$\gamma_\omega(\chi,\tau) \;=\; \sum_{i=1}^{N} a_i(\tau)\psi_i(\chi) \tag{3.25}$$

$$\theta(\chi,\tau) \;=\; \sum_{i=i}^{N} b_i(\tau)\phi_i(\chi) \tag{3.26}$$

where $a_i(\tau)$ and $b_i(\tau)$ are time dependent mode amplitude coefficients.

The polynomial sequence χ^n is used to define the trial functions ϕ. The discretized representation of the polynomial trial function χ^n is generated using the *MWRtool* routine *gdf*. The trial functions are made orthonormal with a numerical Gram-Schmidt orthogonalization routine *gs* . The trial functions for

concentration profile ψ are found as the eigenfunctions of the Sturm-Liouville problem (equation 3.27).

$$\frac{\partial^2 \psi}{\partial \chi^2} = \lambda \psi \tag{3.27}$$

The boundary conditions required to solve the equation using the collocation based Sturm-Liouville solver sl [1] are given by equations (3.28) and (3.29)

$$\psi|_{\chi=1} = 0 \tag{3.28}$$

$$\left.\frac{\partial \psi}{\partial \chi}\right|_{\chi=0} = 0 \tag{3.29}$$

The time derivative functions R_γ (equation 3.30) and R_θ (equation 3.31) are computed by substituting the truncated series expansion approximation into equations (3.12) and (3.13) respectively.

$$
\begin{aligned}
R_\gamma &= D'\nabla_\chi^2(\sum_{i=1}^{N} a_i\psi_i + h\chi^2) - n_0 t_{cycle}(K_f(\sum_{i=1}^{N} a_i\psi_i + h\chi^2)(1 - \sum_{j=1}^{N} b_j\phi_j) \\
&\quad -k_b(\sum_{j=1}^{N} b_j\phi_j)) \tag{3.30}
\end{aligned}
$$

$$
R_\theta = n_0 t_{cycle}(K_f(\sum_{i=1}^{N} a_i\psi_i + h\chi^2)(1 - \sum_{j=1}^{N} b_j\phi_j) - k_b(\sum_{j=1}^{N} b_j\phi_j)) \tag{3.31}
$$

The ∇_χ^2 operator is implemented numerically using a discrete differentiation operator based on Lagrangian interpolation [30]. The functions R_γ and R_θ are projected on the trial functions ψ and ϕ, respectively, to determine the time derivative of the mode amplitude coefficients, a and b. The residual functions are projected on the trial function using overloaded weighted inner product of $tfun$ class.

The Jacobian array of the functions is defined as the derivatives of R_γ and R_θ with respect to the mode amplitude coefficients a and b. Jacobian array is simultaneously projected on the trial functions using a numerical weighted inner

product routine *wip* . The array elements are given by equations (3.32), (3.33), (3.34) and (3.35).

$$
\begin{aligned}
< \frac{\partial R_\gamma}{\partial a_i}, \psi_k > &= D' < \nabla_\chi^2 \psi_i, \psi_k > \\
&\quad -n_0 t_{cycle}(K_f < \psi_i(1 - \sum_{j=1}^{N} b_j \phi_j), \psi_k >) \quad\quad (3.32) \\
< \frac{\partial R_\gamma}{\partial b_j}, \phi_l > &= n_0 t_{cycle}(K_f < (\sum_{i=1}^{N} a_i \psi_i + h\chi^2)\phi_j, \phi_l > \\
&\quad +k_b < \phi_j, \phi_l >) \quad\quad (3.33) \\
< \frac{\partial R_\theta}{\partial a_i}, \psi_k > &= -n_0 t_{cycle} K_f < \psi_i(1 - \sum_{j=1}^{N} b_j \phi_j), \psi_k > \quad\quad (3.34) \\
< \frac{\partial R_\theta}{\partial b_j}, \phi_l > &= -n_0 t_{cycle}(K_f < (\sum_{i=1}^{N} a_i \psi_i + h\chi^2)\phi_j, \phi_l > \\
&\quad +k_b < \phi_j, \phi_l >) \quad\quad (3.35)
\end{aligned}
$$

The initial condition for the mode amplitude coefficients a and b are given by equations (3.36), (3.37), (3.38) and (3.39).

$$
\begin{aligned}
a_i(\tau) &= < \gamma_{desorption}(\tau) - h\chi^2, \psi > \quad \forall \quad \tau = 2n - 1 \quad\quad (3.36) \\
b_i(\tau) &= < \theta_{desorption}(\tau), \phi > \quad \forall \quad \tau = 2n - 1 \quad\quad (3.37) \\
a_i(\tau) &= < \gamma_{adsorption}(\tau) - h\chi^2, \psi > \quad \forall \quad \tau = 2n \quad\quad (3.38) \\
b_i(\tau) &= < \theta_{adsorption}(\tau), \phi > \quad \forall \quad \tau = 2n \quad\quad (3.39)
\end{aligned}
$$

The mode amplitude coefficients are evaluated using a polynomial collocation based ODE/AE solver *odaepc* [23]. The concentration and fractional site occupancy profiles of the gaseous species, computed using the above numerical technique are in close agreement with the published result [16]. The concentration and the fractional site occupancy profiles for the case of pure diffusion, unsaturated reaction and saturated reaction are plotted in figures (3.4), (3.5) and (3.6) respectively.
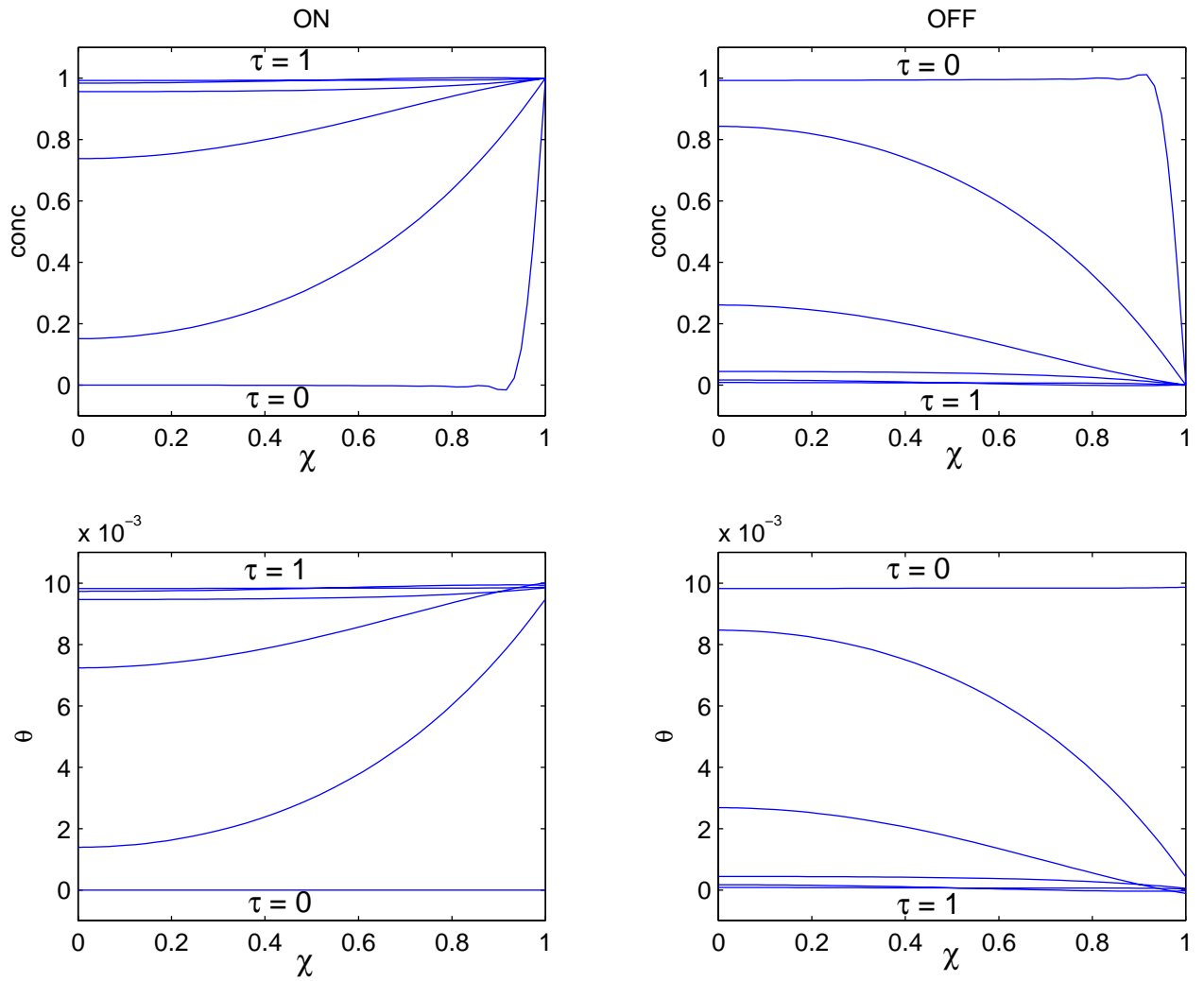
Figure 3.4: Concentration and fractional site occupancy profiles during adsorption (ON) and desorption (OFF) cycle for case of pure diffusion of gas in polymer film.
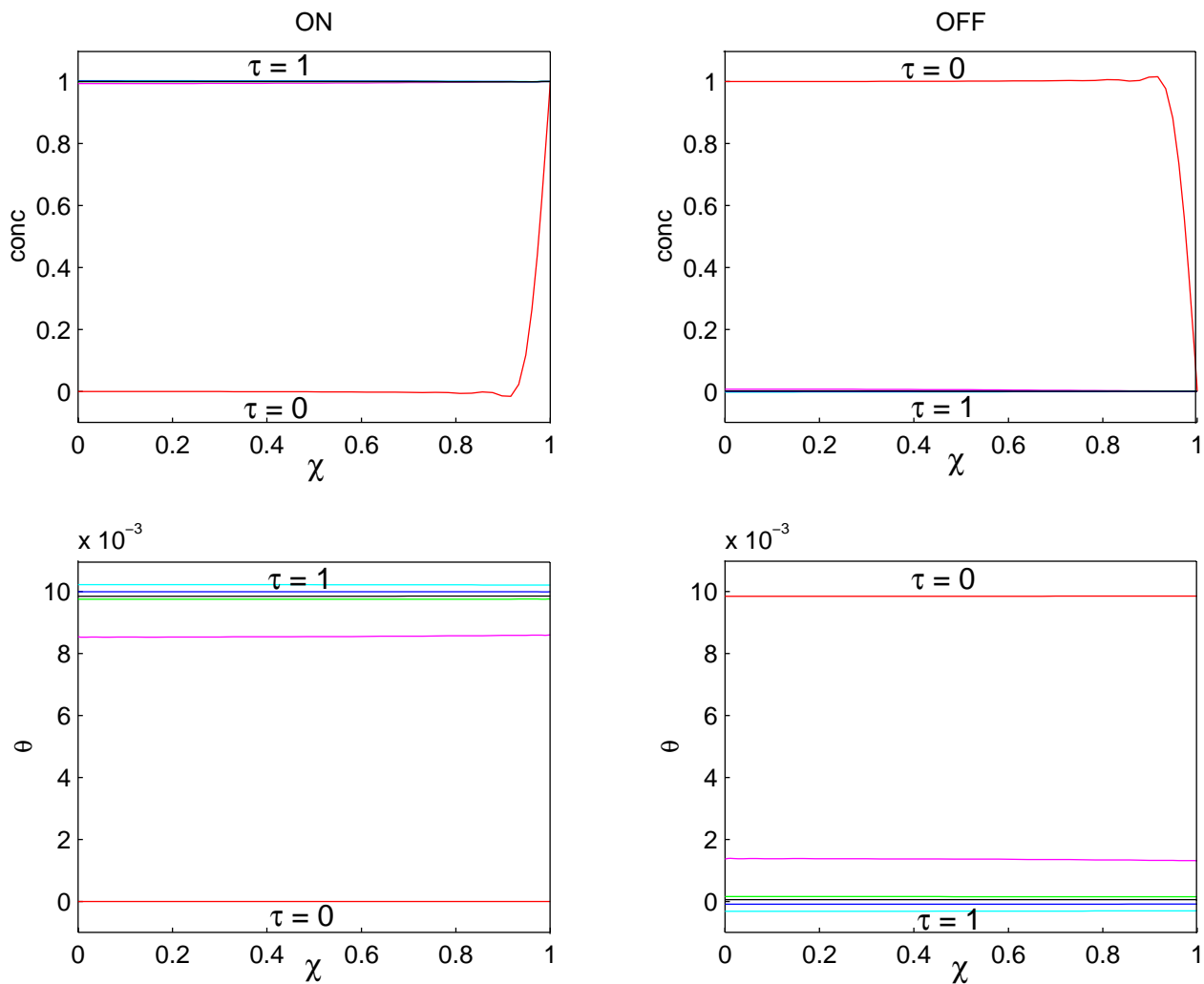
Figure 3.5: Concentration and fractional site occupancy profiles during adsorption (ON) and desorption (OFF) cycle for the case of unsaturated reaction of a gas with the polymer film.
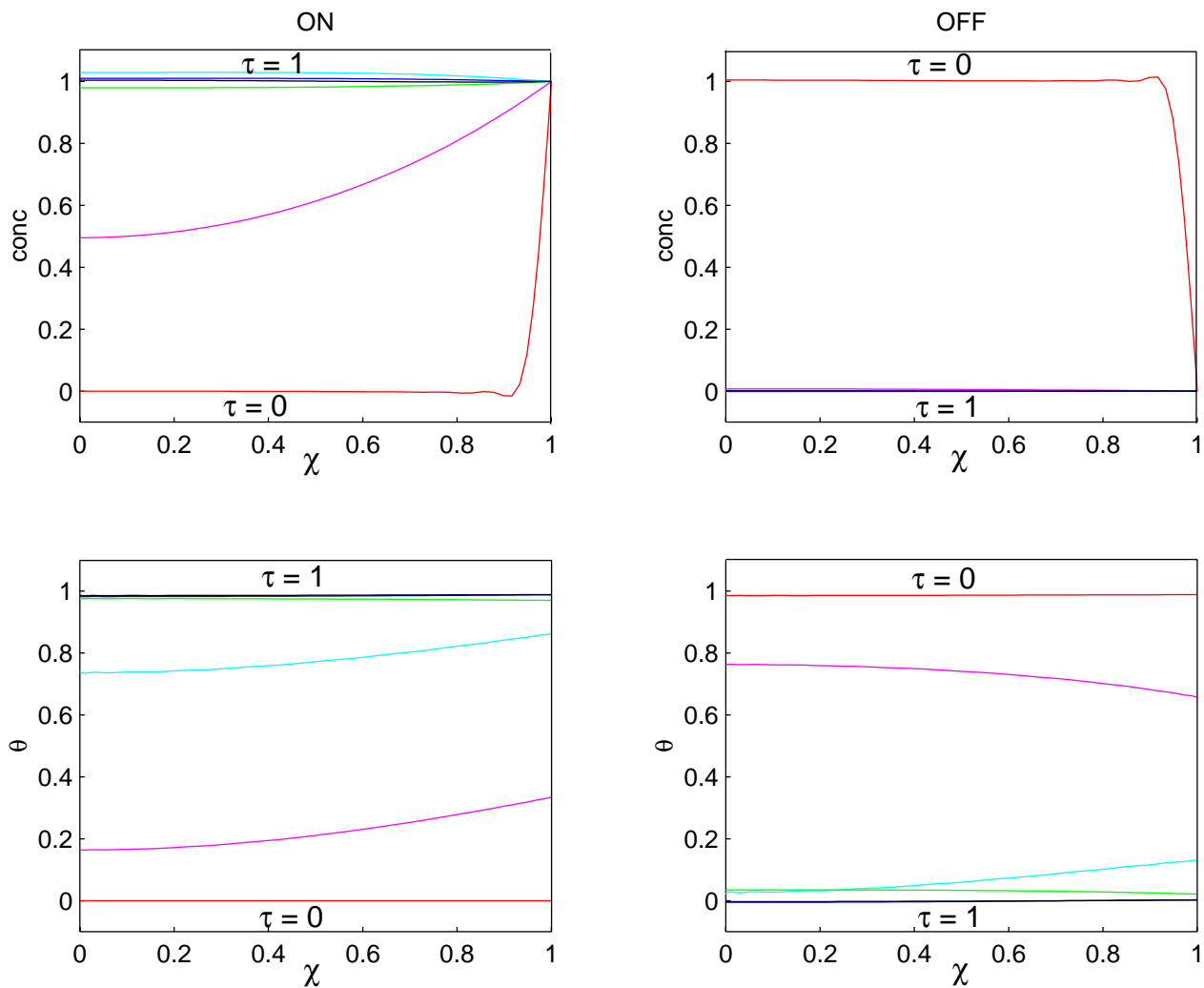
Figure 3.6: Concentration and fractional site occupancy profiles during adsorption (ON) and desorption (OFF) cycle for the case of saturated reaction of a gas with the polymer film.

3.4   Device conductance model

The conducting polymer can be represented as a 3-dimensional, randomly distributed array of N identical resistive links. Each link represents a barrier to the movement of electrons from one conjugated polymer backbone onto another. As per the conductance response mechanism, an adsorbed gas molecule modifies a certain number n of the resistive links. There are $n\theta$ links of resistance R_{filled} and $(N$ - $n\theta)$ links of resistance R_0. The macroscopic resistance of such a system is determined in the way we connect up the N resistors.

In the circuit theoretic approach for deriving the electrical properties of statistical mixture [9][10] the resistors are arranged in square network as shown in figure (3.7). Each node of the network is made up of six other resistors, which are referred to as node resistors (figure 3.8). The resistors represent the possible connection with other monomers converging on the node. In each node no more than two of the six connections can be enabled at a time.

The model is simplified to resistors connected in parallel. Film conductivity $\sigma(\chi,\tau)$ is linearly related to the site occupancy (equation 3.40 and 3.41).

$$\sigma(\chi,\tau) = \sigma_0[1 - S^{/}\theta(\chi,\tau)] \tag{3.40}$$

$$\sigma(\chi,\tau) = \sigma_0 - S\theta(\chi,\tau) \tag{3.41}$$

where $S^{/}$ is the gas sensitivity coefficient of the polymer and σ_0 is the conductivity of the sensor in absence of gas in the polymer film.

Coplanar thin electrodes and semi-infinite electrode geometry are commonly used in gas sensors. In the case of semi-infinite thin electrode the electric field bisecting the electrodes has been determined using the Schwartz-Christoffel trans-
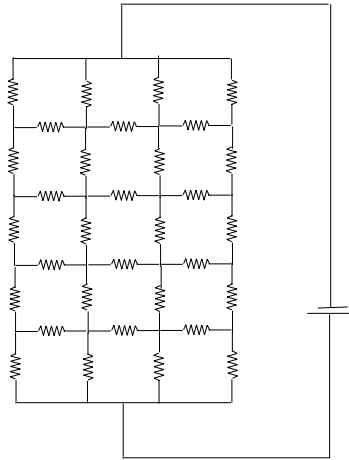
Figure 3.7: Schematic diagram of square mesh network model.
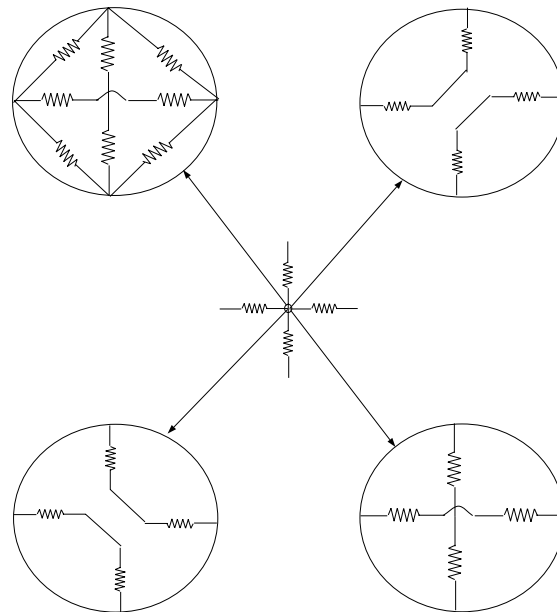
Figure 3.8: Schemes of short-circuit connections allowed at each node.

formation [19] as given in equation (3.42).

$$E_a(\chi, \tau) = \frac{\frac{V}{L\pi}}{\sqrt{(\chi^2 + \frac{w^2}{4L^2})}} \tag{3.42}$$

where V is the voltage applied across the electrodes and w is the width between the electrodes. The fractional change in conductance of the sensor is given by equation (3.43).

$$\frac{G_\tau - G_0}{G_0} = \frac{\sigma_\tau - \sigma_0}{\sigma_0} = -S\frac{\int_0^1 \frac{\theta(\chi,\tau)}{\sqrt{(\chi^2+(\frac{w}{2L})^2)}}d\chi}{ln[\frac{1+\sqrt{(1+(\frac{w}{2L})^2)}}{\frac{w}{2L}}]} \tag{3.43}$$

The electric field for a pair of finite coplanar thin electrodes of width d is given by equation (3.44).

$$E_b(\chi,0) = \frac{V}{2A^*L^2}\frac{1}{\sqrt{([\chi^2 + (\frac{w}{2L})^2)][M^2\chi^2 + (\frac{w}{2L})^2]}} \tag{3.44}$$

where M is the geometric modulus $(\frac{w}{w+2d})$ and the constant A^* is determined from the complete elliptical integral (equation 3.45).

$$A^* = \frac{2}{w}\int_0^1 \frac{dt^*}{\sqrt{(1-t^2)(1-(Mt^*)^2)}} \tag{3.45}$$

The sensor's response (i.e. fractional change in conductance) for the coplanar electrode can be calculated as shown in equation (3.46).

$$\frac{G_\tau - G_0}{G_0} = \frac{\sigma_\tau - \sigma_0}{\sigma_0} = -S\frac{\int_0^1 \frac{\theta(\chi,\tau)d\chi}{\sqrt{(\chi^2+(\frac{w}{2L})^2)(M^2\chi^2+(\frac{w}{2L})^2)}}}{\int_0^1 \frac{d\chi}{\sqrt{(\chi^2+(\frac{w}{2L})^2)(M^2\chi^2+(\frac{w}{2L})^2)}}} \tag{3.46}$$

3.5   Parameter estimation

The physical properties of the polymer depend on the polymerization process used for the synthesis of the gas sensor. Slight change in any parameter during

31

polymerization drastically affects the properties of the polymers. Therefore, it is nearly impossible to accurately calculate the properties using empirical formulae or published results. However, they do serve as a good initial guess for parameter estimation.

The rate of diffusion (D) of gaseous species in the polymer, rate of adsorption (k_f) and desorption reaction (k_b) of the gaseous species and gas sensitivity coefficient of the polymer (S) must be estimated using the experimental data. The parameters estimated using the optimization toolbox of $MATLAB$ are tabulated in table (3.1). Additional parameters required for the computation are given in table (3.2). The steps involved in optimization of parameter values are outlined in figure (3.9). The objective function to be minimized is defined as the sum of squares of the error between the model predictions and experimental measurements. The latter was obtained from [27] by digitizing the plots using the image processing toolbox of $MATLAB$.

Table 3.1: Estimated Parameters

	NO_x	NH_3
K_f	0.006094	0.04637
k_b	0.005709	0.05586
S	-0.8878e6	5.8134e6
D	11.186e-14	8.1815e-14

The modeling equations are numerically integrated over two adsorption/desorption cycles using collocation-based ODE/AE solver to obtain the concentration and fractional site occupancy profiles. The simulated values are available at collo-
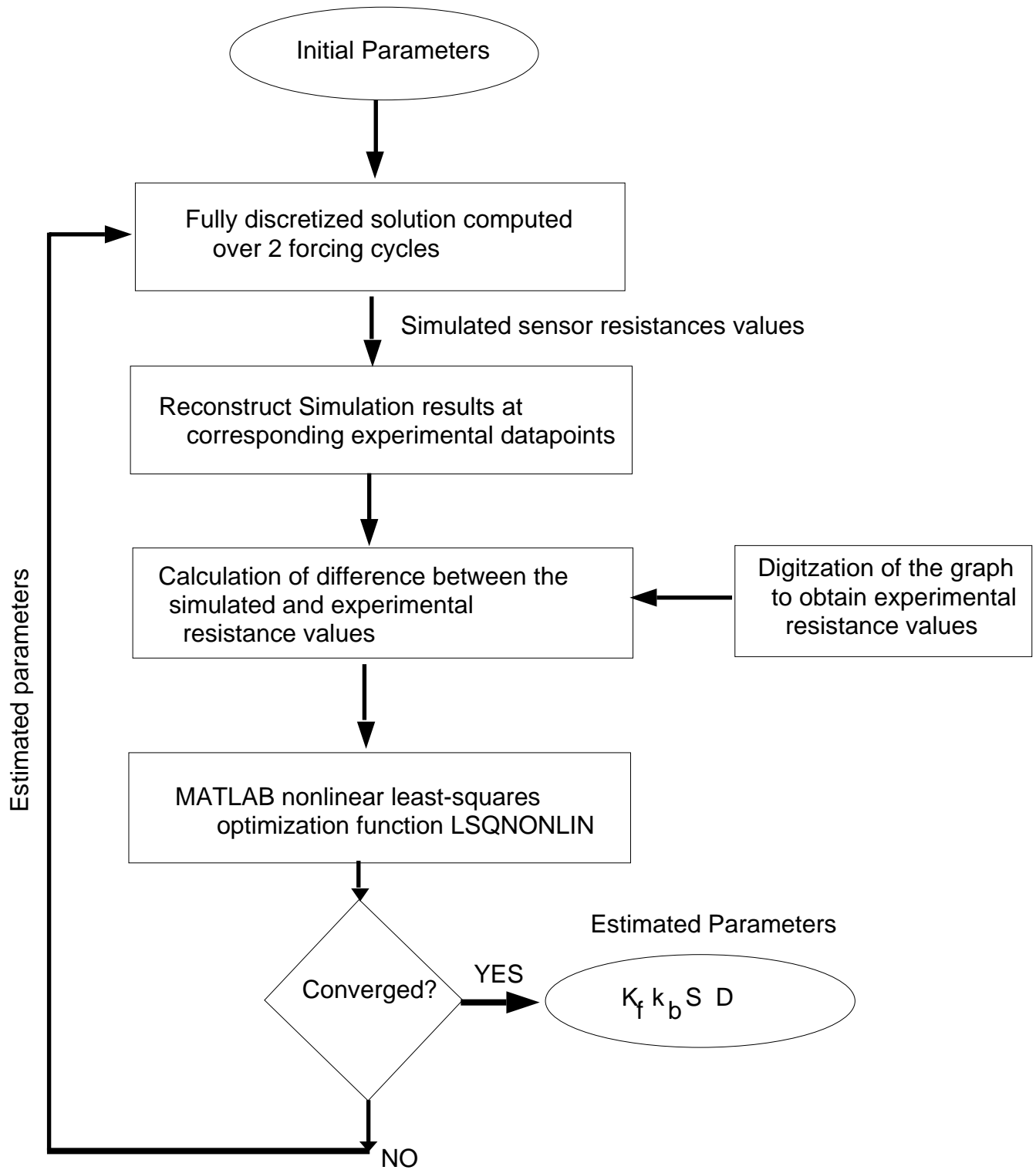
Figure 3.9: Steps involved in optimization of parameter values.

Table 3.2: Additional Parameters

Parameters	Values
Thickness of sensor	1e-5m
Dimensionless site density	1
Time constant	241sec
Spatial discretization points	40
Collocation points in time	6
Base resistance for NO_x	1.2e6
Base resistance for NH_3	4.7e6

cation points in time, and are reconstructed at the points in time at which the experimental values are available using the polynomial basis functions of the collocation procedures. The resistance values are calculated from the fractional site occupancy profile using the device conductance model. The optimal set of parameters are computed until the difference between the experimental and simulated values are less than 1% of the experimental value.

3.6 Sensitivity with respect to discretization parameters

In order to estimate the parameters to model the adsorption of NO_x gas in the conducting polymer, initially the modeling equations were numerically integrated over single adsorption/desorption cycle. The PDE's were solved using 28 quadrature points along the length of the polymer film and six collocation points in time.

Eight eigenfunctions were computed using the Sturm-Liouville solver. Eight trial functions were used for computing concentration and fractional occupancy profiles (figure 3.10). The parameters obtained on optimization are tabulated in table (3.3). The comparison of the experimental and simulated resistance values for one adsorption and desorption cycles are plotted in figure (3.11).

Table 3.3: Initial Estimated Parameters for NO_x gas.

K_f	0.1797
k_b	0.0297
S	-0.4927e6
D	9.7701e-14

The PDE's were solved with greater number of collocation points in time and it was found that similar results were obtained. The number of points along the length of the polymer film was increased to 40. 16 eigenfunctions were computed using the Sturm-Liouville solver. The concentration and fractional occupancy profiles are plotted in figure (3.12). The simulated resistance values are plotted in figure (3.13). Fractional site occupancy shoots above 100, whereas the acceptable values are in the range 0-1. The concentration varies between 3.5 and -8. The dimensionless concentration should lie in the range 0-1. Resistance of the sensor has a negative value, when only positive values are accepted. Increasing the number of points should have improved the solution rather than leading to instability. Hence it is essential to perform sensitivity analysis to verify the presence of global minima and accurate estimation of parameters.

The optimization was performed with 40 discretization points in space. The
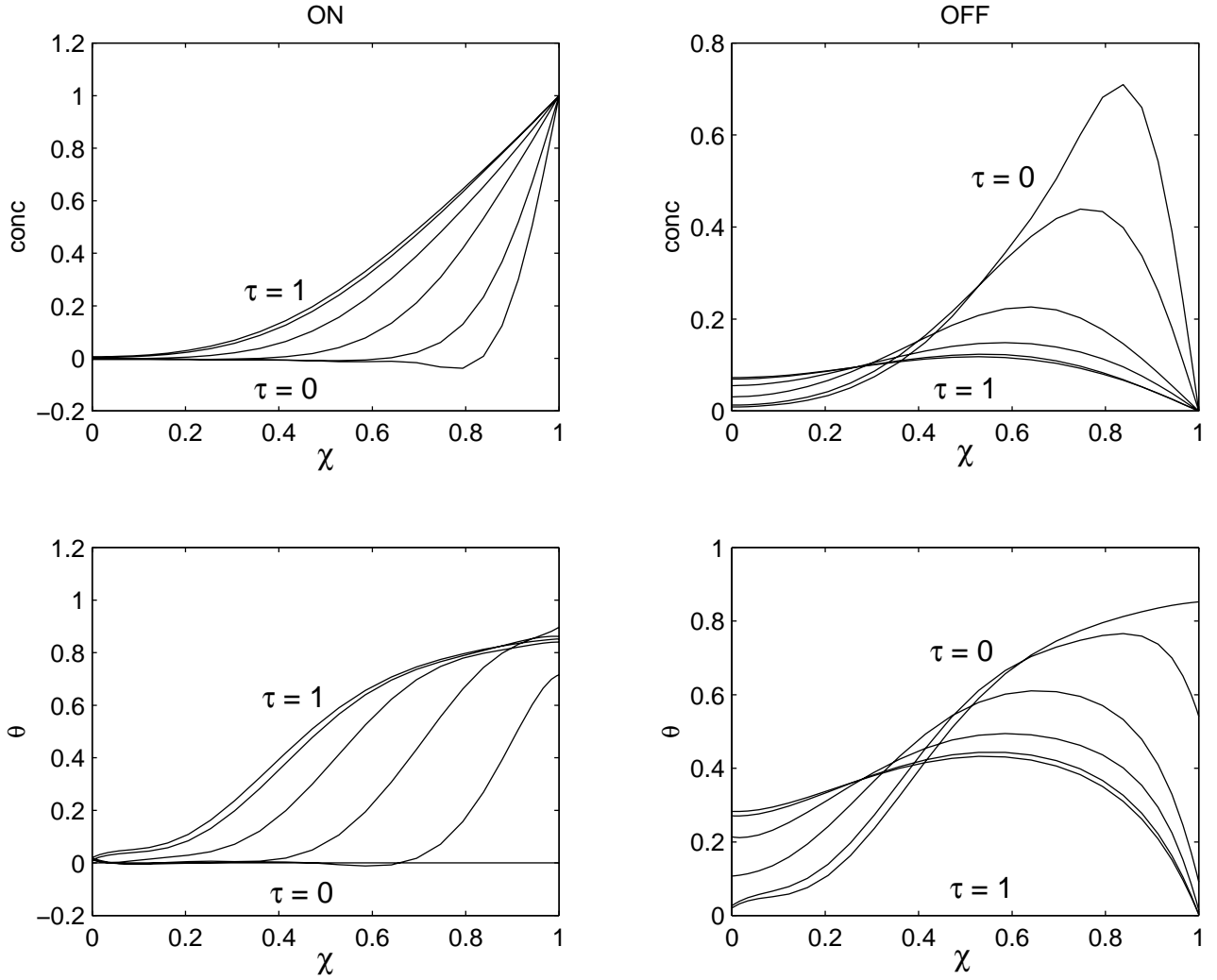
Figure 3.10: Concentration and fractional occupancy profile computed using eight trial functions for parameters which are optimal but do not converge for higher number of trial functions.
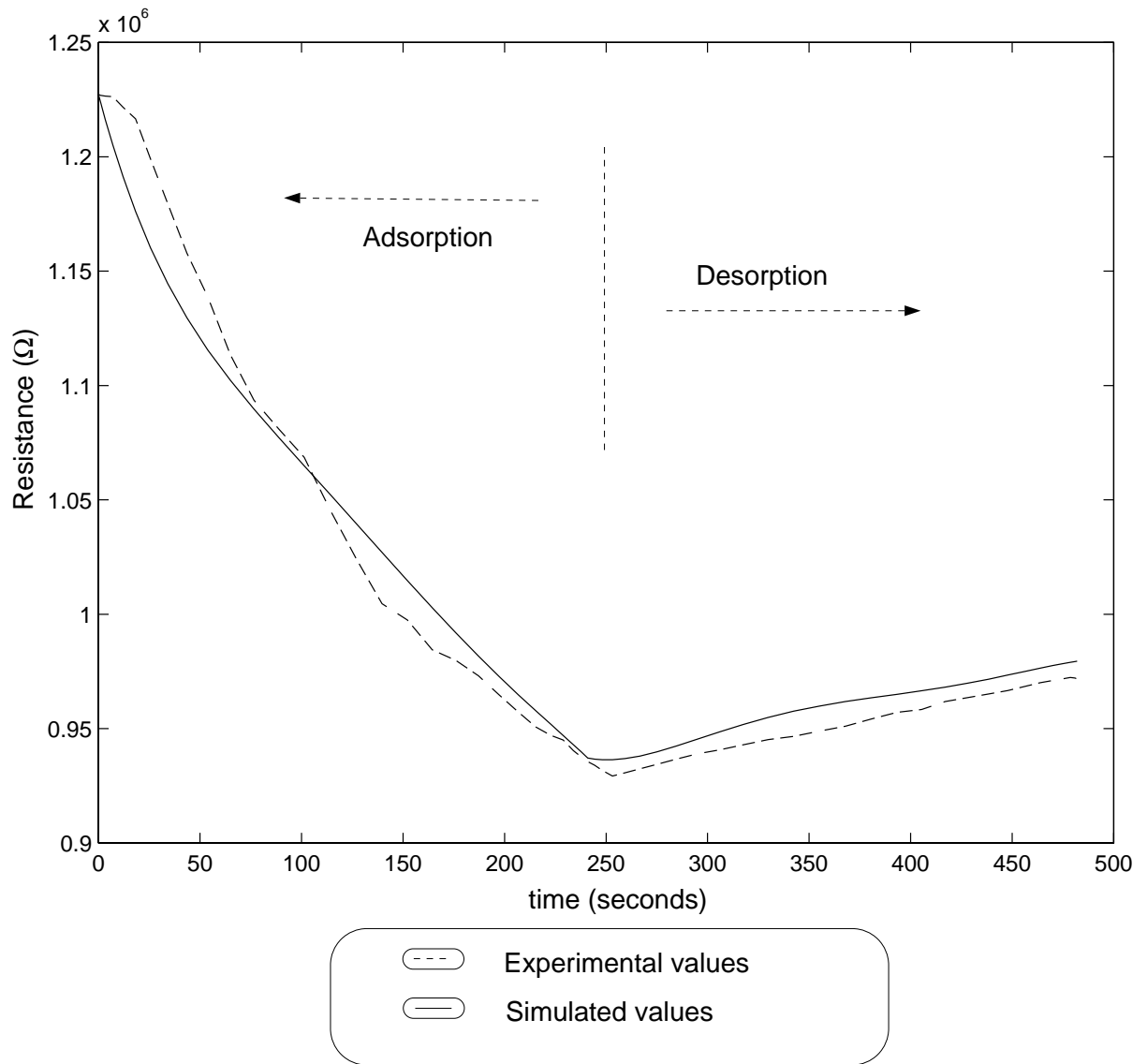
Figure 3.11: Comparison of experimental and simulated resistance profiles for NO_x computed using eight trial functions for parameters which are optimal but do not converge for higher number of trial functions.
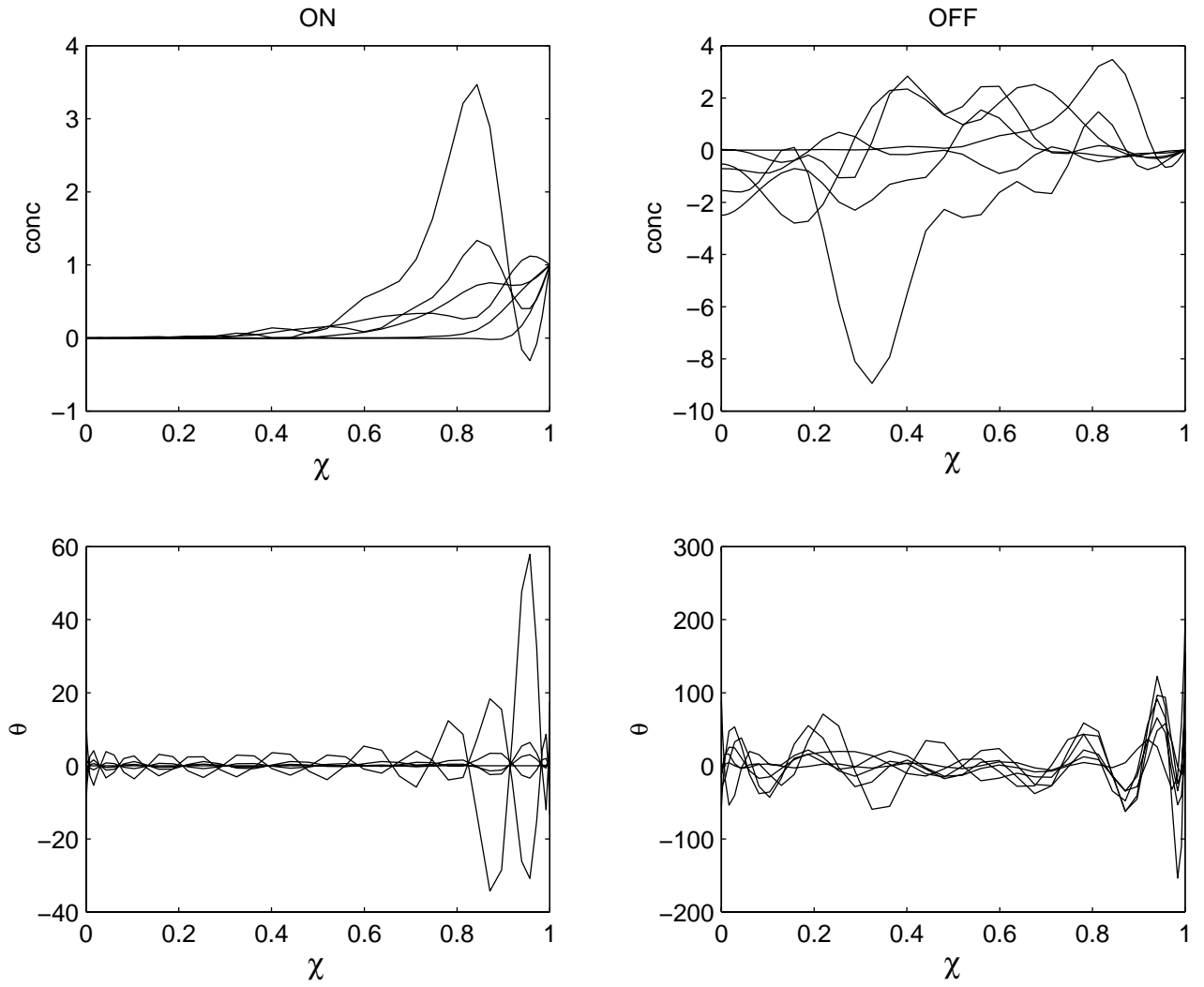
Figure 3.12: Concentration and fractional occupancy profiles computed using sixteen trial functions for parameters which are optimal but do not converge for higher number of trial functions.
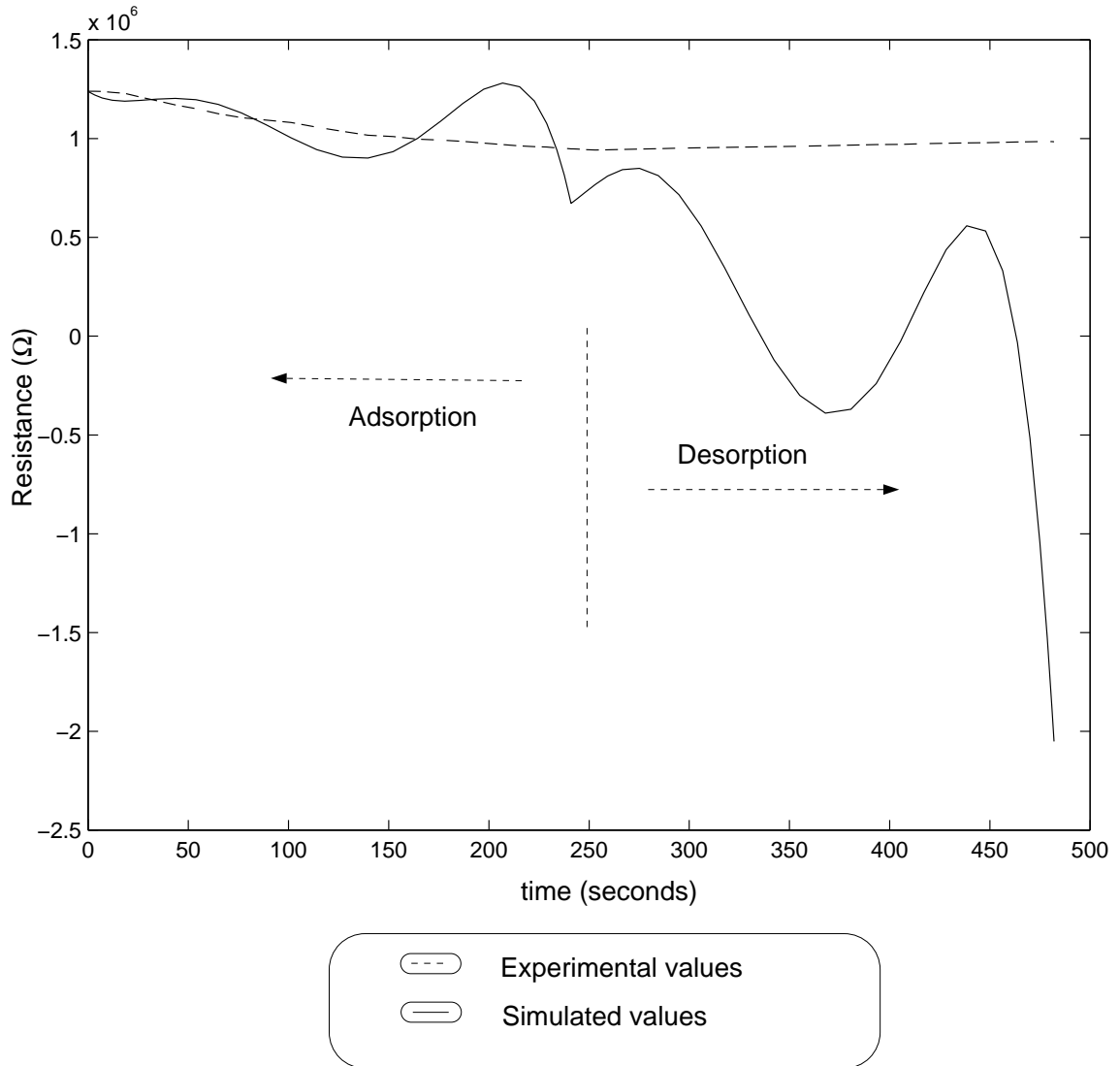
Figure 3.13: Comparison of experimental and simulated resistance profiles for NO_x computed using sixteen trial functions for parameters which are optimal but do not converge for higher number of trial functions.

Table 3.4: Local optimal parameters for NO_x gas

K_f	0.0579
k_b	0.0059
S	-0.31e6
D	19.81e-14

modeling equations were numerically integrated over two adsorption/desorption cycles. The optimal values for the parameters are tabulated in table (3.4). There is a good match between the simulated and experimentally obtained resistance values for the initial two adsorption and desorption cycles as shown in figure (3.14). However the simulated resistance values do not drift in the subsequent cycles in contrast with the experimental values. The analysis of the concentration and fractional occupancy profiles (figure 3.15) reveal that the polymer film is saturated with gas. Hence, the resistance does not drift in the subsequent cycles. There is a difference of order of magnitude between the rate of adsorption and desorption of gas, which leads to saturation. The optimization is repeated with different sets of initial parameters, which lead to globally optimal solution. Concentration and fractional occupancy profiles are plotted in figure (3.16). The comparison of the experimental and simulated resistance values is plotted in figure (3.17).

In case of ammonia gas, increasing the number of collocation points in space and time improved the solution marginally, therefore, we consider these solution to be converged. Initial parameter guesses were also varied as part of the identification procedure to verify that the parameters were global minima rather than

Table 3.5: Sensitivity with respect to estimated parameters for NH_3 gas

Initial Guesses

K_f	0.1253	0.0313	0.05	0.07518
k_b	0.1243	0.0310	0.0497	0.07457
S	10.044e6	2.511e6	4.0176e6	6.0264e6
D	17.084e-14	4.271e-14	6.8336e-14	10.044e-14

Optimal parameters

K_f	0.04295	0.04431	0.04428	0.04432
k_b	0.05090	0.05406	0.05403	0.05409
S	5.8632e6	5.8587e6	5.8590e6	5.8590e6
D	8.189e-14	8.192e-14	8.192e-14	8.193e-14

local minima. The initial guess and the final set of parameters for NH_3 are given in table 3.5.

3.7 Results and discussion

The concentration and fractional occupancy ratio profile snapshots for six collocation points in time for adsorption (ON) and desorption (OFF) in first and sixth cycle are recorded in figures (3.18) and (3.19) respectively. The figures (3.18) and (3.19) indicate the amount of gas remaining in the conducting polymer film after desorption cycle. The gaseous species may not desorb completely even if it was not exposed to gaseous species for long period of time. Hence more efficient desorption techniques like heating are required for cleaning the sensor of the gaseous
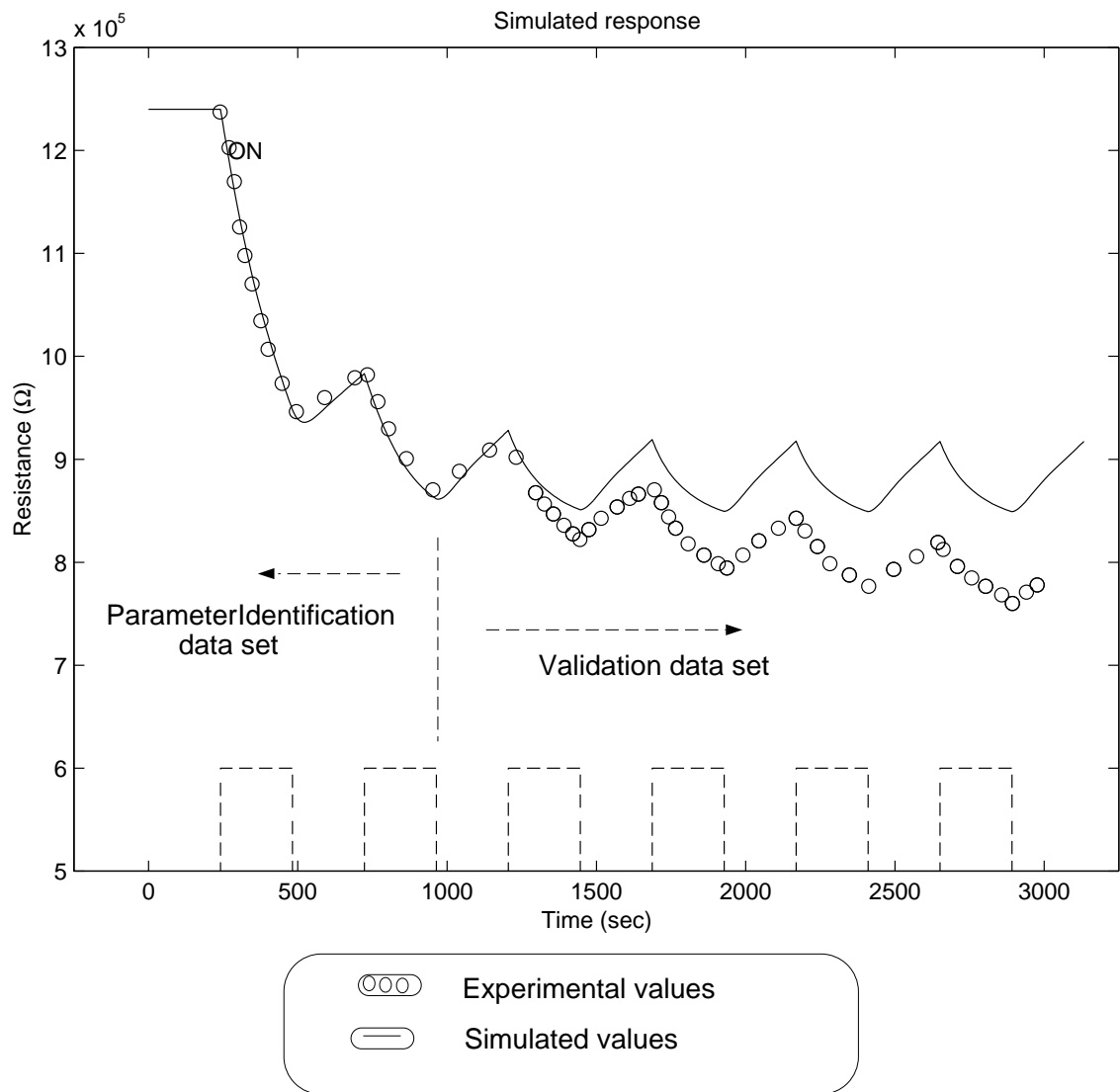
Figure 3.14: Comparison of experimental and simulated resistance profiles for NO_x using local optimal parameters.
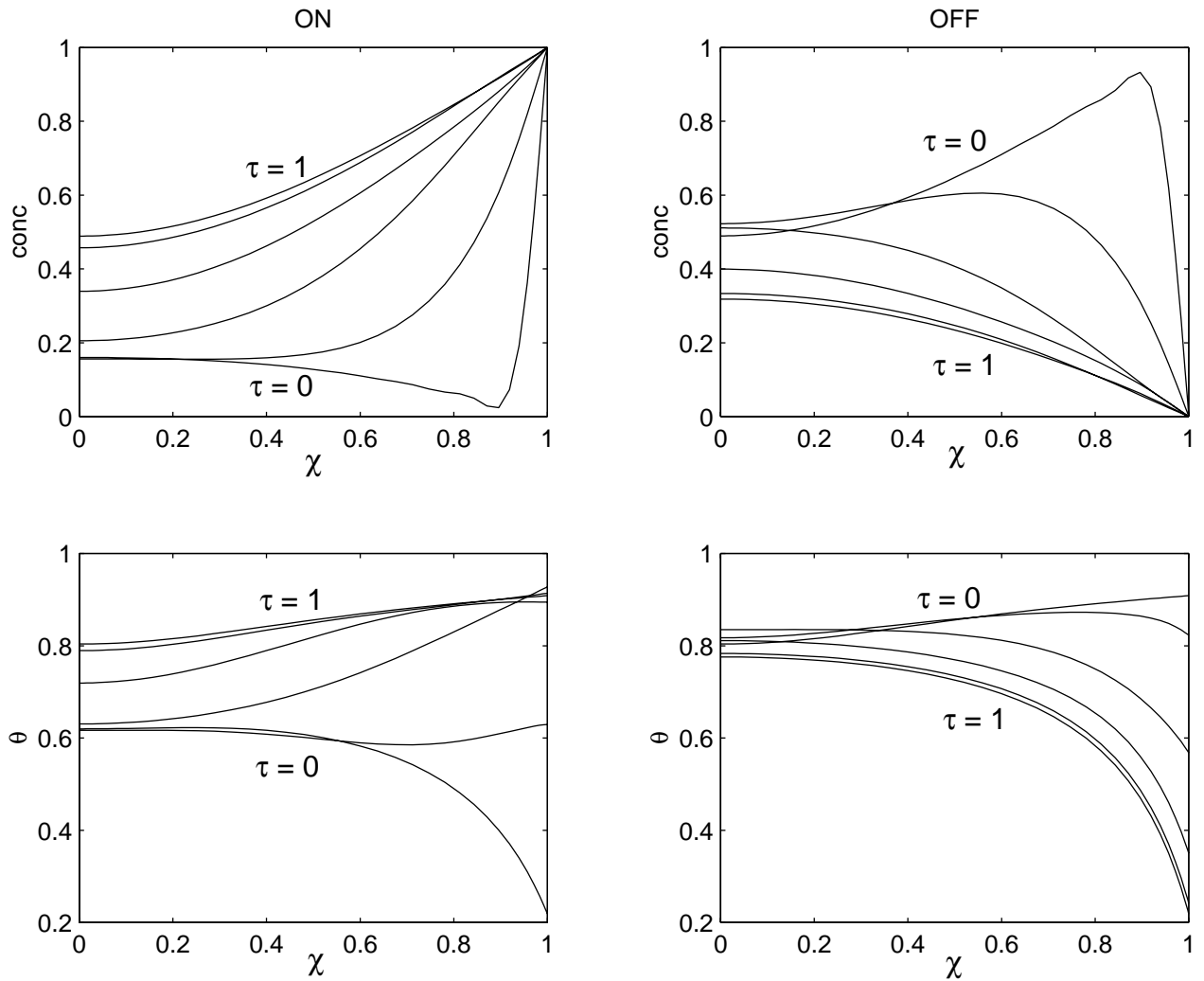
Figure 3.15: Concentration and fractional occupancy profiles for NO_x gas using local optimal parameters.
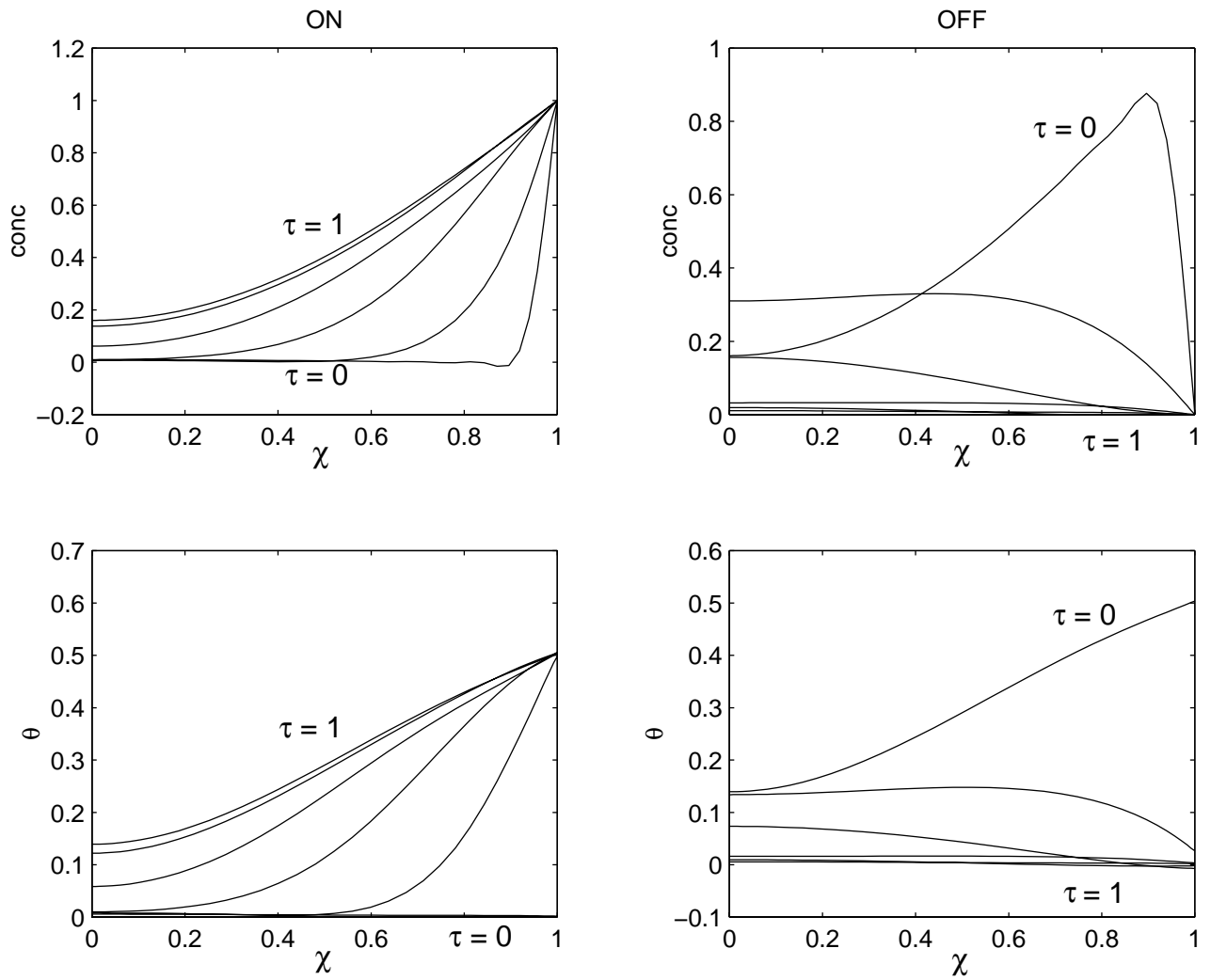
Figure 3.16: Concentration and fractional occupancy profiles for NO_x gas using globally optimal parameters.
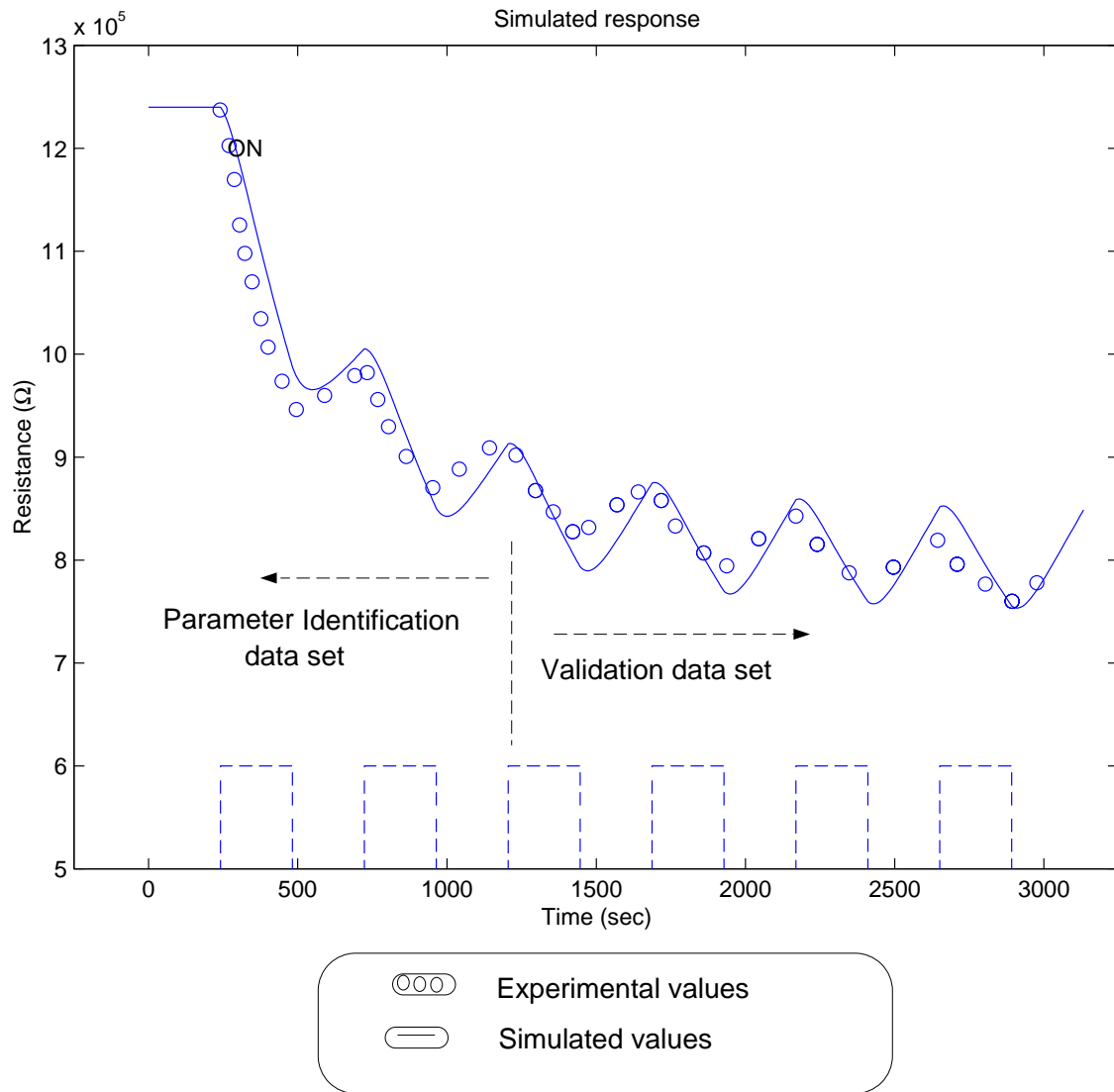
Figure 3.17: Comparison of experimental and simulated resistance profiles for NO_x using globally optimal parameters.

species.

The change in concentration and fractional site occupancy is negligible in approximately 40% of the sensor film in the sixth cycle as seen in figure (3.19). The amount of gas adsorbed in the polymer film in the sixth cycle is much less than that adsorbed in the first cycle. Since the change in the conductivity of the conducting polymer depends on amount of gas adsorbed, sensitivity of the sensor is reduced in the subsequent cycles.

The experimental and simulated resistance profiles of NO_x and NH_3 gas are compared in figures (3.17) and (3.20) respectively. The dotted square wave represents gas flow above the surface of the polymer film. The unconnected zeros represent experimental values while simulated values are drawn as a dotted curve. There is a good match between the resistance values obtained experimentally and those predicted by the model.

The resistance increases in case of NH_3 gas and decreases in the case of NO_x gas. NH_3 is a reducing gas. It donates electrons and reduces the number of charge carriers namely bipolarons. Hence conductivity of the polymer film decreases and resistance increases. NO_x is an oxidizing gas and hence reverse effects are observed. Resistance decreases and conductivity increases. Thus the results are in conformation with the theory of conductance.

The base resistance of the sensor drifts in the subsequent cycles. This drift in resistance is due to improper cleaning of gases during the desorption cycle. The difference in the resistance values in each cycle decreases as the number of cycle increases. This indicates that the sensitivity of the sensor decreases. This is in conformation with the results obtained from concentration and fractional site occupancy profiles.
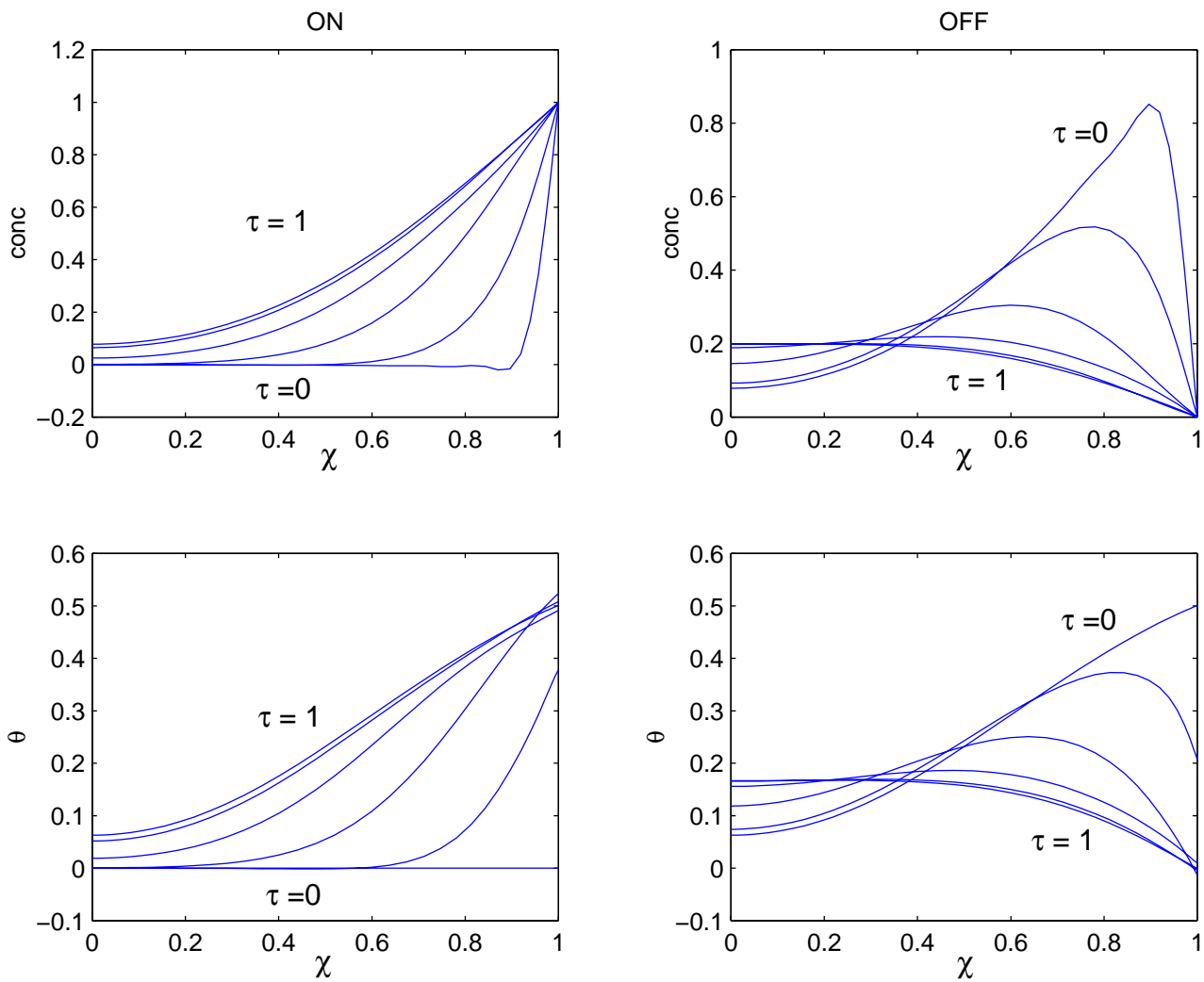
Figure 3.18: Concentration and fractional site occupancy profiles during adsorption (ON) and desorption (OFF) cycle of NH_3 in polymer film of isothermal sensor during the first cycle.
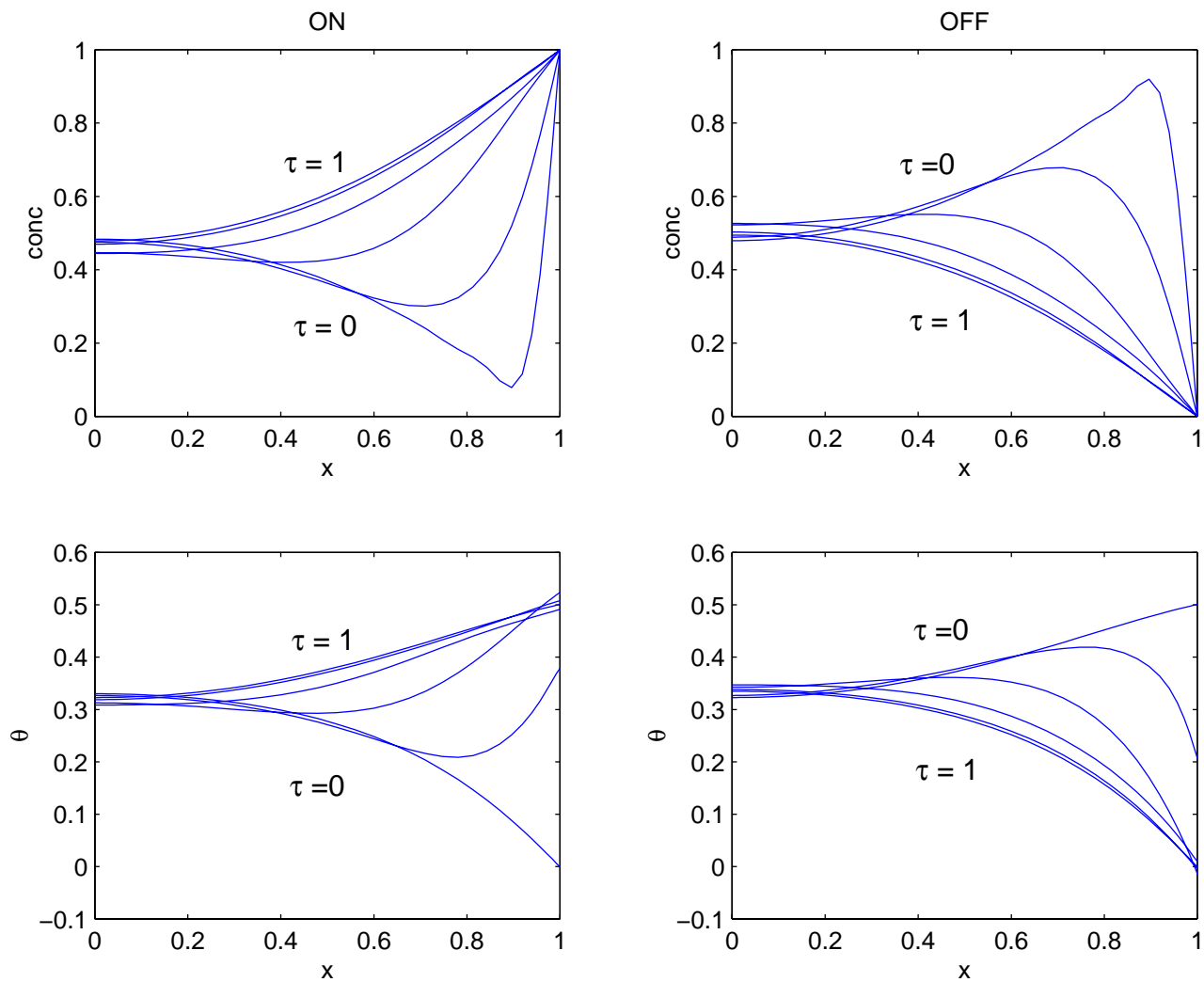
Figure 3.19: Concentration and fractional site occupancy profiles during adsorption (ON) and desorption (OFF) cycle of NH_3 in polymer film of isothermal sensor during the sixth cycle.
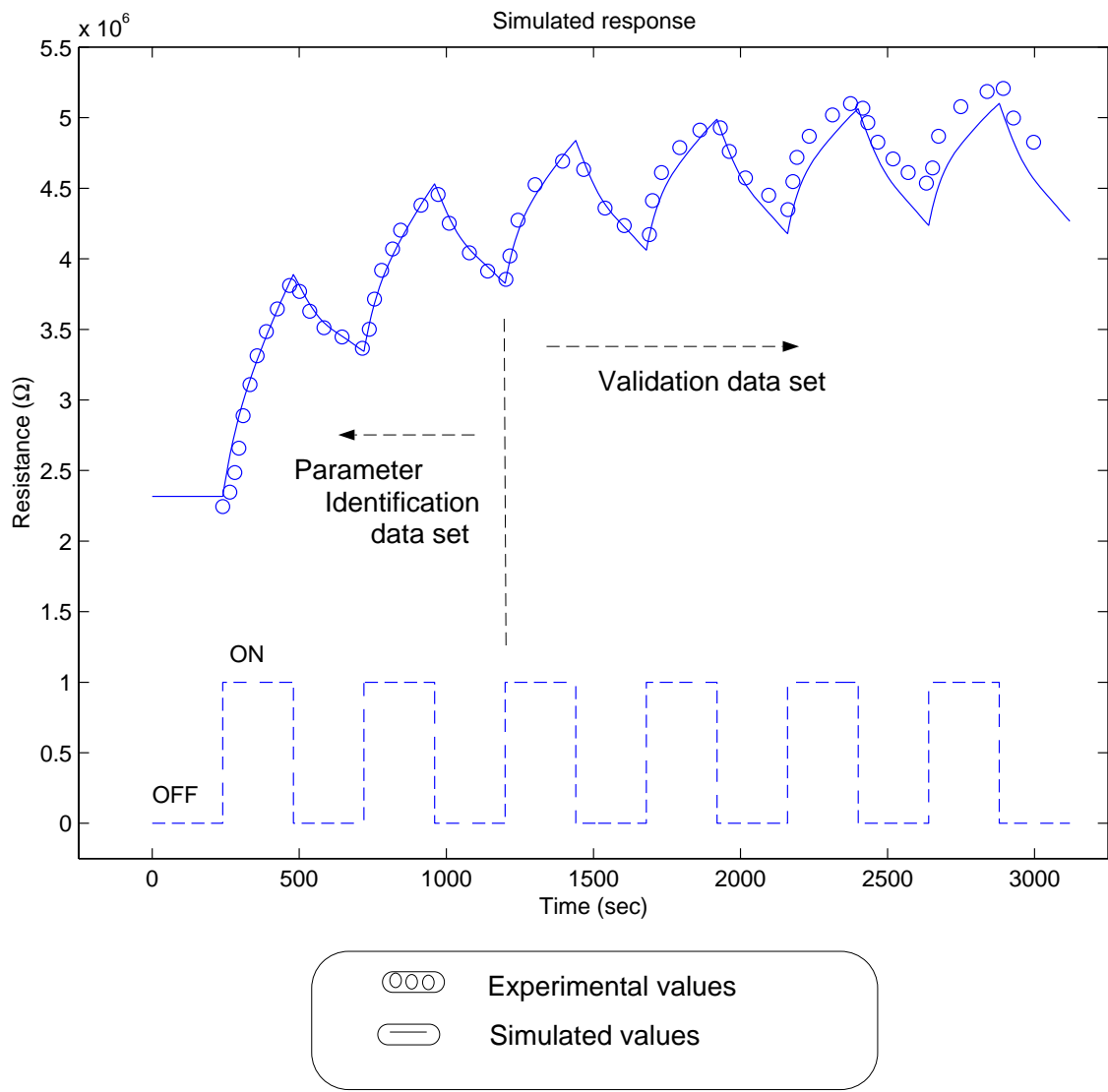
Figure 3.20: Comparison of experimental and simulated resistance profiles for NH_3.

Chapter 4

Microhotplate based gas sensor

4.1 Introduction

Gas species may not be driven out of the polymer film completely during desorption if the conducting polymer sensor is operated at ambient temperature. This leads to a drift in the base resistance of the sensor. Additionally, lesser amount of gas diffuses into the film during the subsequent adsorption cycle. Presence of gas in the polymer decreases the effective sensitivity of the sensor. Moisture and gases also react with the π bonds of the pyrrole ring and cause irreversible changes, leading to the degradation of the polymer.

It could take infinite time for the gas to desorb completely from the polymer film. Hence, efficient sensor cleaning techniques are necessary. In batch mode, the sensors are cleaned using a solvent, which dissolves the gases [18]. However this cannot be implemented for online gas analysis. The rate of diffusion, adsorption and desorption of gases in the conducting polymer increase with temperature. Gas would desorb completely if the sensor is operated at elevated temperature during the process of desorption. This would enable maximum reproducible sensitivity and baseline recovery following gas exposure.
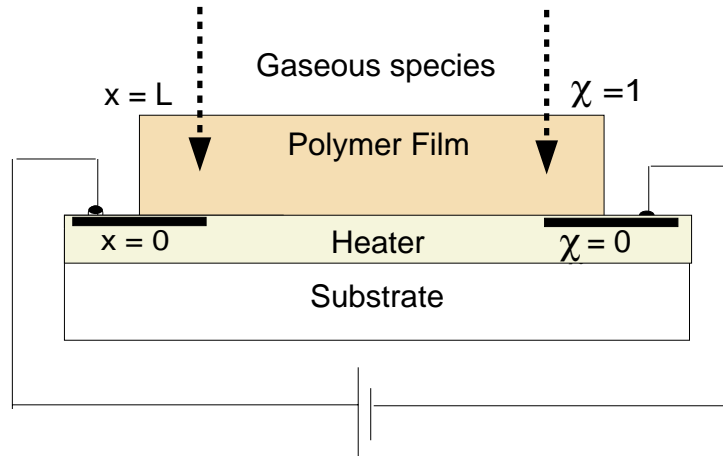
Figure 4.1: Schematic diagram of the micro-hotplate gas sensor.

Researchers at National Institute of Standards and Technology (NIST) have developed a new generation of conducting polymer gas sensors namely, conductometric micro-hotplate gas sensor [28][37]. The schematic diagram is given in figure (4.1). The sensor consists of a multidimensional array of micro-hotplate elements fabricated on a single section of a single wafer. Each sensor element has multiple layers as shown in figure (4.2). The base element of the gas sensor is designed at NIST and fabricated by a commercial CMOS (Complimentary Metal Oxide Semiconductor) technology such as the metal oxide semiconductor implementation service (MOSIS). The bottom layer consists of an individually addressable heater. A metal hotplate layer is employed for heat distribution and temperature measurement and four top-level contact pads allow the conductance measurement. All the layers are insulated by SiO_4 passivation masks. Pits are etched under the suspended heater structure to provide thermal insulation from surrounding substrate. The thermal isolation and low mass of the micro-bridge

enable control of individual temperature without altering the temperature of the surrounding. Conducting polymer can be deposited using electro-polymerization or Langmuir Blodgett technique.
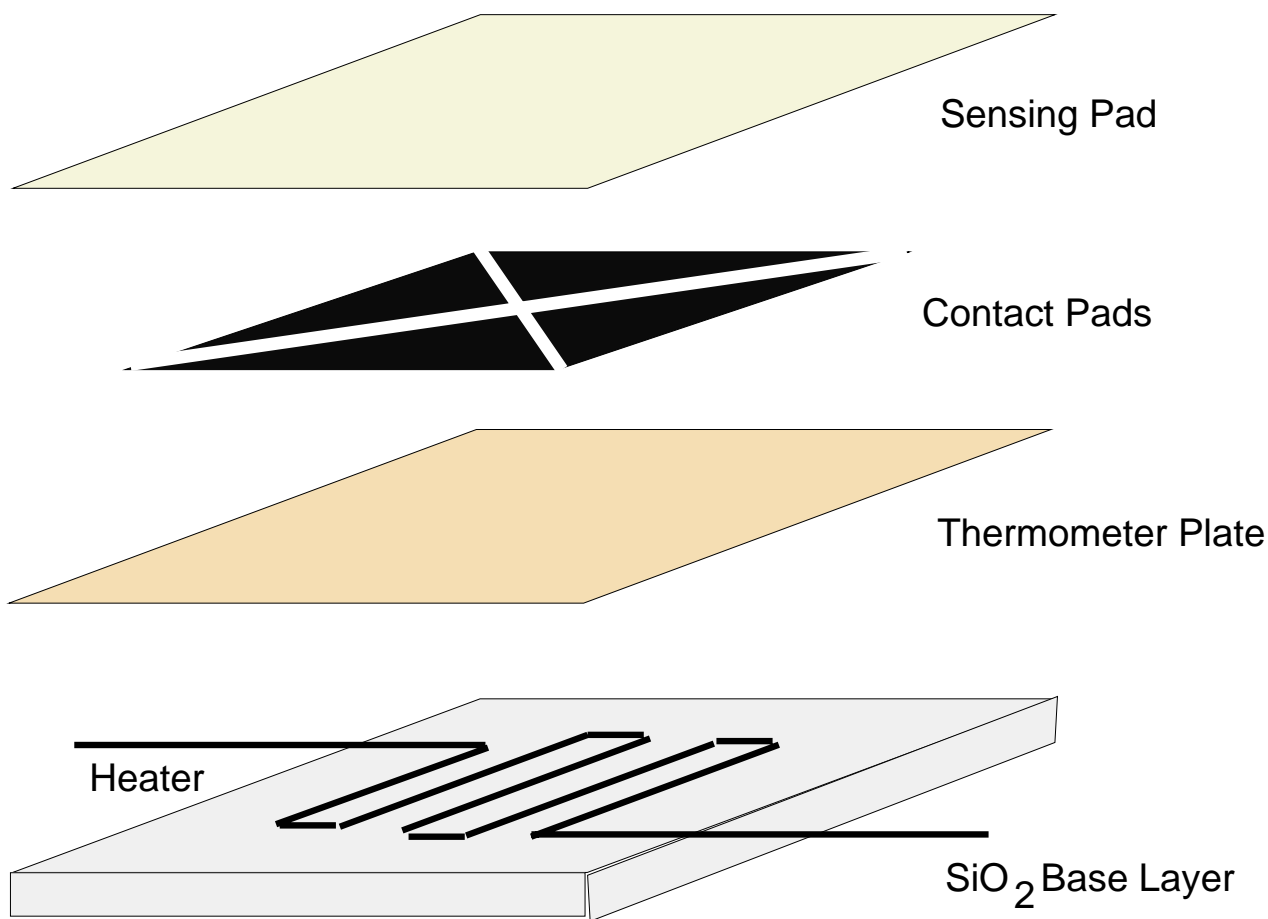
Figure 4.2: Multilevel view of the Micro hotplate.

4.2   Modeling of polymer film temperature profile

The micro-hotplate is kept at ambient temperature (T_0) during adsorption. During desorption, the heater is switched on and the temperature of the polymer

film is increased to temperature (T_{high}). T_{high} is lower than the decomposition temperature and glass transition temperature of the conducting polymer.

Temperature distribution in the polymer film is obtained by considering the energy balance in polymer film and applying the Fourier law of heat conduction (equation 4.1).

$$\frac{\partial T}{\partial t} = \alpha \frac{\partial^2 T}{\partial x^2} \tag{4.1}$$

where α is the thermal diffusivity of conducting polymer.

We assume that the micro-hotplate and the surface of the polymer film in contact with micro-hotplate ($x = 0$) attain temperature (T_p) immediately. The temperature of the film in contact with the hotplate is given by equation (4.2).

$$
\begin{aligned}
T|_{x=0} &= T_p \\
&= T_0 + (T_{high} - T_0)b(t) \tag{4.2}
\end{aligned}
$$

where $b(t)$ is a square wave of unit amplitude and time period same as adsorption/desorption cycle time. The surface of the polymer film in contact with the air ($x = L$) loses heat by convection. The rate of conduction of heat in the polymer film at the polymer film/gas interface ($x = L$) is equal to loss of heat to the gas (equation 4.3).

$$k\frac{\partial T}{\partial x} - h(T - T_0)\bigg|_{x=L} = 0 \tag{4.3}$$

Initially the polymer film is kept at ambient temperature T_0. For subsequent adsorption and desorption cycles, the concentration at the end of the previous cycle serves as the initial condition (equations 4.4 and 4.5).

$$
\begin{aligned}
T_{desorption}(t) &= T_{adsorption}(t) \quad \forall \quad t = T_{cycle}(2n-1) \tag{4.4} \\
T_{adsorption}(t) &= T_{desorption}(t) \quad \forall \quad t = T_{cycle}(2n) \tag{4.5}
\end{aligned}
$$

The dimensionless temperature(Θ) and thermal diffusivity ($\alpha^{'}$) are given by equations (4.6) and (4.7) respectively.

$$\Theta = \frac{T - T_0}{T_{high} - T_0} \tag{4.6}$$

$$\alpha^{'} = \frac{\alpha t_{cycle}}{L^2} \tag{4.7}$$

The dimensionless length (χ), time (τ), thermal diffusivity ($\alpha^{'}$) and temperature (θ) is substituted into the continuity equation, boundary conditions and initial conditions to obtain equation (4.8), (4.9), (4.10), (4.11) and (4.12).

$$\frac{\partial \Theta}{\partial \tau} = \alpha^{'} \frac{\partial^2 \Theta}{\partial \chi^2} \tag{4.8}$$

$$\Theta|_{\chi=0} = b(\tau) \tag{4.9}$$

$$k \frac{\partial \Theta}{\partial \chi} - h\Theta|_{\chi=1} = 0 \tag{4.10}$$

$$\Theta_{desorption}(\tau) = \Theta_{adsorption}(\tau) \quad \forall \quad \tau = 2n - 1 \tag{4.11}$$

$$\Theta_{adsorption}(\tau) = \Theta_{desorption}(\tau) \quad \forall \quad \tau = 2n \tag{4.12}$$

4.3 Numerical solution

The dimensionless differential equations, boundary conditions and initial conditions are discretized and solved using Galerkin's method similar to the procedure used for solving concentration and fractional site occupancy profiles.

The dimensionless temperature is defined by equation (4.13).

$$\Theta = \Theta_\omega + \Theta_{\partial\omega}$$
$$= \Theta_\omega + \Theta_0(\tau)(1 - \chi)^2 \tag{4.13}$$

As per the Galerkin discretization procedure, component of the dimensionless temperature which satisfy the homogeneous boundary condition (Θ_ω) is expressed

in terms of the orthogonal function expansion (ζ) (equation 4.14).

$$\Theta_\omega(\chi, \tau) = \sum_{i=1}^{M} c_i(\tau)\zeta_i(\chi) \tag{4.14}$$

The trial functions for concentration profile ζ_i are the eigenfunctions of the Sturm-Liouville equation (equation 4.15).

$$\frac{\partial^2 \zeta}{\partial \chi^2} = \delta\zeta \tag{4.15}$$

subject to homogeneous boundary conditions given by equations (4.16) and (4.17).

$$\zeta|_{\chi=0} = 0 \tag{4.16}$$

$$k\frac{\partial \zeta}{\partial \chi} - h\zeta\Big|_{\chi=1} = 0 \tag{4.17}$$

Substituting the truncated series expansion approximation into equation (4.8) forms the semi discretized form of the modeling equation (equation 4.18).

$$R_\Theta = \alpha^{'}\nabla_\chi^2(\sum_{i=1}^{M} c_i\zeta_i + \Theta_0(1-\chi)^2) \tag{4.18}$$

The function R_Θ is projected on the trial functions ζ to obtain the same number of algebraic equations as the number of mode amplitude coefficients. Each element of the Jacobian array necessary for the collocation-based time integrator is given by equation (4.19).

$$< \frac{\partial R_\Theta}{\partial c_i}, \zeta_k > = \alpha^{'} < \nabla_\chi^2\zeta_i, \zeta_k > \tag{4.19}$$

The initial condition for the mode amplitude coefficient c_i are given by equation (4.20) and (4.21).

$$c_{i,adsorption}(\tau) = < \Theta_{desorption}(\tau) - \Theta_0(1-\chi)^2, \zeta_i > \ \forall \ \tau = 2n-1 \tag{4.20}$$

$$c_{i,desorption}(\tau) = < \Theta_{adsorption}(\tau) - \Theta_0(1-\chi)^2, \zeta_i > \ \forall \ \tau = 2n \tag{4.21}$$

4.4 Temperature response

The parameter values in addition to those used for simulation of concentration profiles are listed in table (4.1). Temperature response is very fast as compared to the concentration response, hence approximate value of the parameters serve the purpose.

Table 4.1: Parameters for simulating temperature profile

Parameters	Values
Thermal diffusivity	7.5e-5 $\frac{m^2}{sec}$
Thermal conductivity	0.15 $\frac{J}{sec.m.K}$
heat-transfer coefficient	0.2 $\frac{J}{sec.m^2.K}$
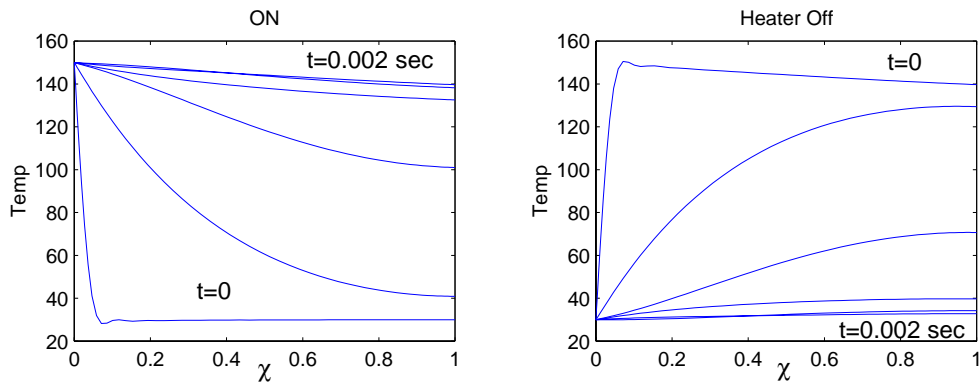
Figure 4.3: Temperature profile during adsorption (OFF) and desorption (ON).

The temperature profile along the length of the sensor is plotted in figure (4.3). The figure on the left corresponds to temperature profile when the heater is switched ON. The change in temperature of the polymer film is very fast as compared to the diffusion of the gas in the conducting polymer. The response time of

temperature is in order of milliseconds while the time for adsorption/desorption of gas in polymer sensor is approximately 241 sec. Hence we can assume that during desorption of gases from the conducting polymer, the temperature remains constant at the elevated temperature. Temperature during adsorption is the ambient temperature (T_0). Hence the modeling equations for the concentration profile and the fractional site occupancy remain the same as those in the isothermal case. In the isothermal case the same set of parameters were applicable for the adsorption/desorption cycle. However due to temperature dependence of the parameters, two sets of parameters, one each for the adsorption and desorption cycle, are required. The Arrhenius rate law gives the temperature dependence of the rates of forward and backward adsorption reaction (equation (4.22) and (4.23)).

$$k_f = k_{f0} exp\left(\frac{E_f}{RT}\right) \tag{4.22}$$

$$k_b = k_{b0} exp\left(\frac{E_b}{RT}\right) \tag{4.23}$$

where E_f and E_b are the activation energies of the adsorption and desorption respectively.

The Mott's variable range hopping model (VRH) gives the temperature dependence of the conductivity of the polymer film [11]. The sensitivity coefficient of the polymer to the gas follows similar temperature dependence as the conductivity (equation (4.24)).

$$\sigma = \sigma_0 exp\left(\left(\frac{T_0}{T}\right)^{0.25}\right) \tag{4.24}$$

4.5 Parameter estimation

The temperature remains constant during desorption and adsorption cycle at T_{high} and T_0 respectively. The rate of diffusion (D) of gaseous species in the polymer, rate of adsorption (K_f) and desorption reaction (k_b) of the gaseous species and gas sensitivity coefficient of the polymer (S) are estimated at both temperatures. The estimated values, given in table (4.2), are as expected from the theory of temperature dependence. The rate of the adsorption and desorption increases as expected from Arrhenius equation. The resistance of the conducting polymer decreases and the sensitivity coefficient increases as expected from the VRH.

Table 4.2: Estimated Parameters for NH_3 gas

	Adsorption	Desorption
K_f	1.77e-2	33e-2
k_b	1.74e-2	67e-2
S	2.21e6	5.02e6
D	1.17e-13	9.40e-13

4.6 Result and discussion

The concentration and fractional occupancy ratio profile snapshots for six and twenty collocation points in time for adsorption (ON) and desorption (OFF) of the gas in the conducting polymer at elevated temperature in first cycle is recorded in figures (4.4) and (4.5) respectively.
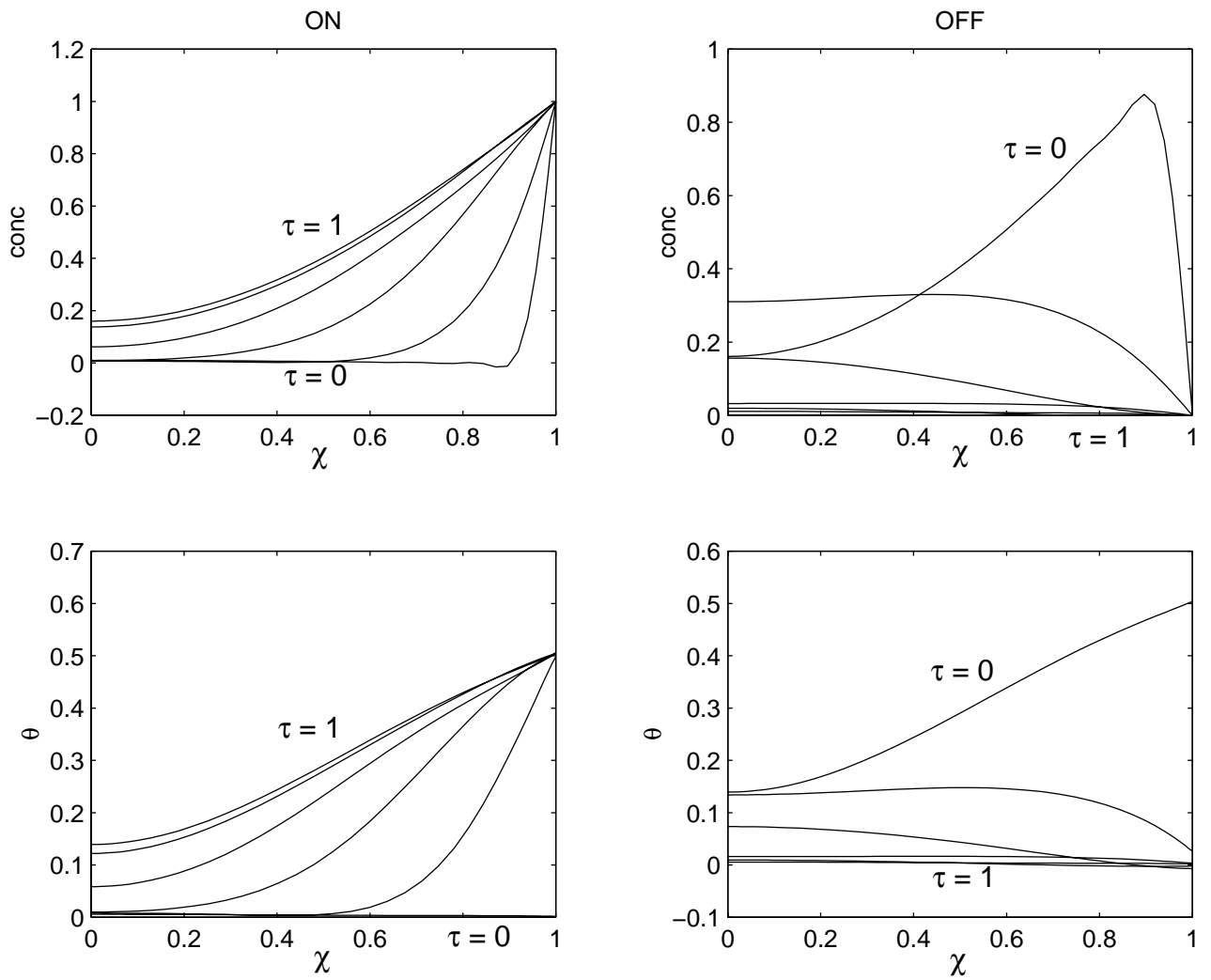
Figure 4.4: Concentration profile and fractional occupancy profiles during adsorption and desorption of NH_3 gas using six collocation points in time.
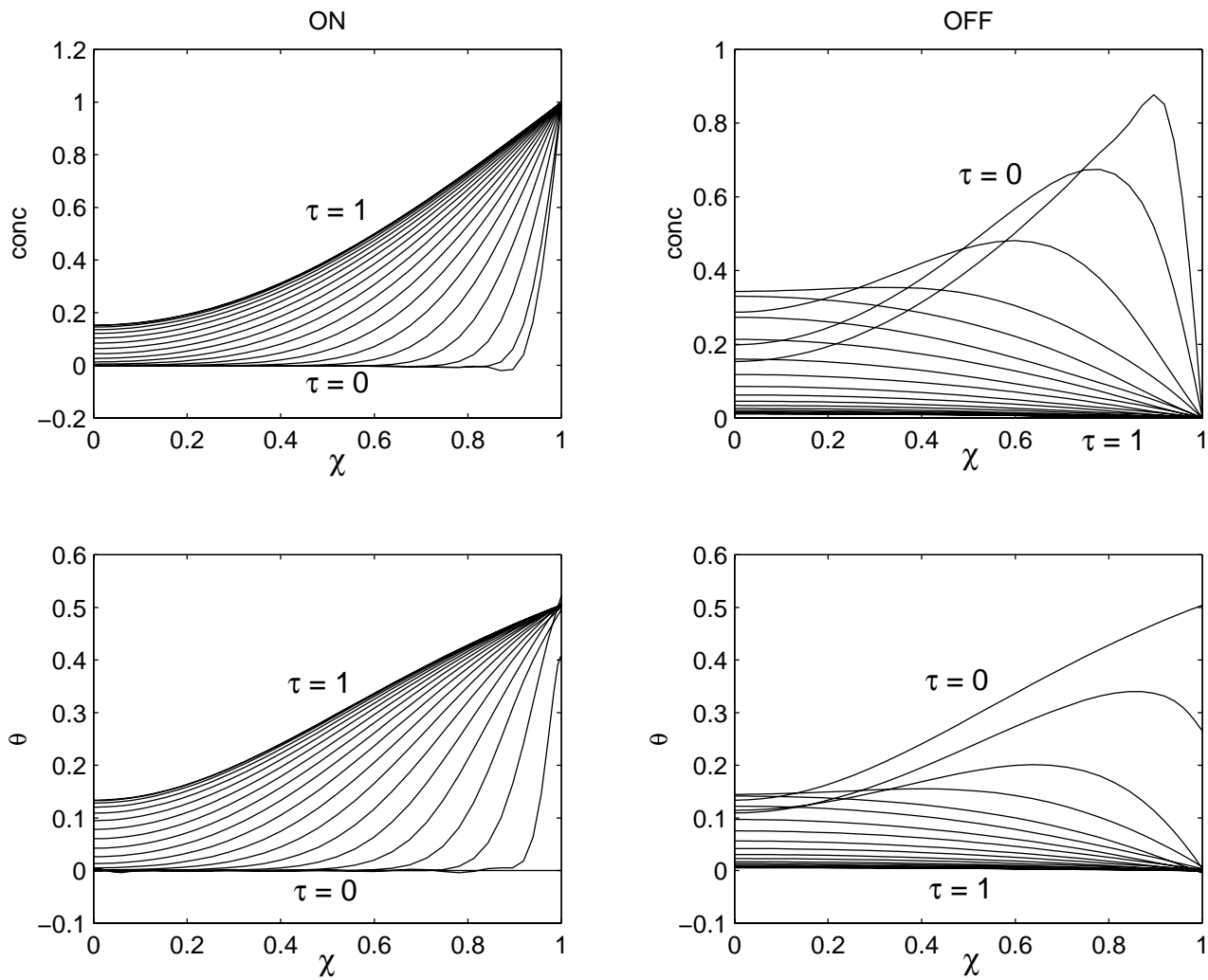
Figure 4.5: Concentration profile and fractional occupancy profiles during adsorption and desorption of gaseous species using twenty collocation points in time.

The concentration of the gas in the conducting polymer at the end of desorption cycle is shown in figure (3.19). The polymer film was maintained at ambient temperature during desorption cycle. The initial concentration for subsequent adsorption cycle is greater than zero. This leads to a drift in the base resistance. The sensitivity also decreases because a lesser amount of gas is adsorbed. However, the concentration of the gas in the conducting polymer during desorption at elevated temperature essentially reaches zero. Time required for desorption of gaseous species is reduced. This can improve the response time of the sensor.

The figures (4.6) and (4.7) compare the experimental and simulated resistance profiles for the case of NH_3 gas. Six collocation points in time are used to integrate the PDE's in the earlier case and twenty collocation points are used in the latter case. The dashed curve represents simulated resistance values for microhotplate based gas sensor while experimental values are drawn as unconnected circles. The bold curve represents the resistance values predicted by isothermal model.

If six collocation points in time are used for computing the concentration and fractional occupancy profile, the resistance decreases initially and then rises and decreases eventually. This leads to a formation of bump, in contrast to experimentally obtained resistance values.

There is reversal of diffusion of gas into the film during desorption. This would mean that six collocation points in time were not enough to reflect the changes in fractional occupancy profile. On increasing the number of collocation points in time to 20, the minor changes in fractional occupancy could be noted and the resultant resistance shows a constant decrease in the resistance, which matches with the experimental results.
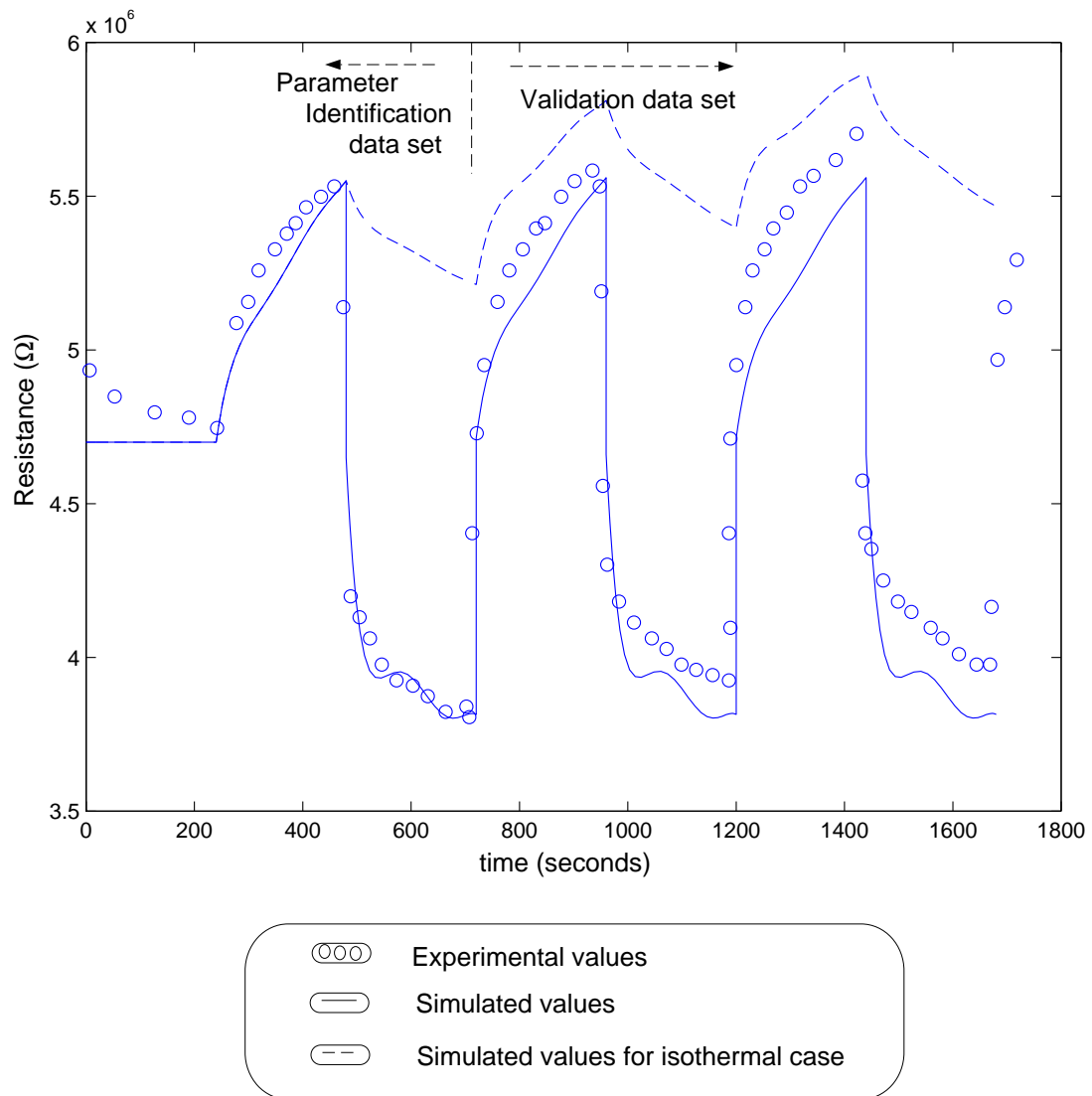
Figure 4.6: Comparison of experimental and simulated resistance profiles of micro-hotplate based sensor for NH_3 gas using six collocation points in time.
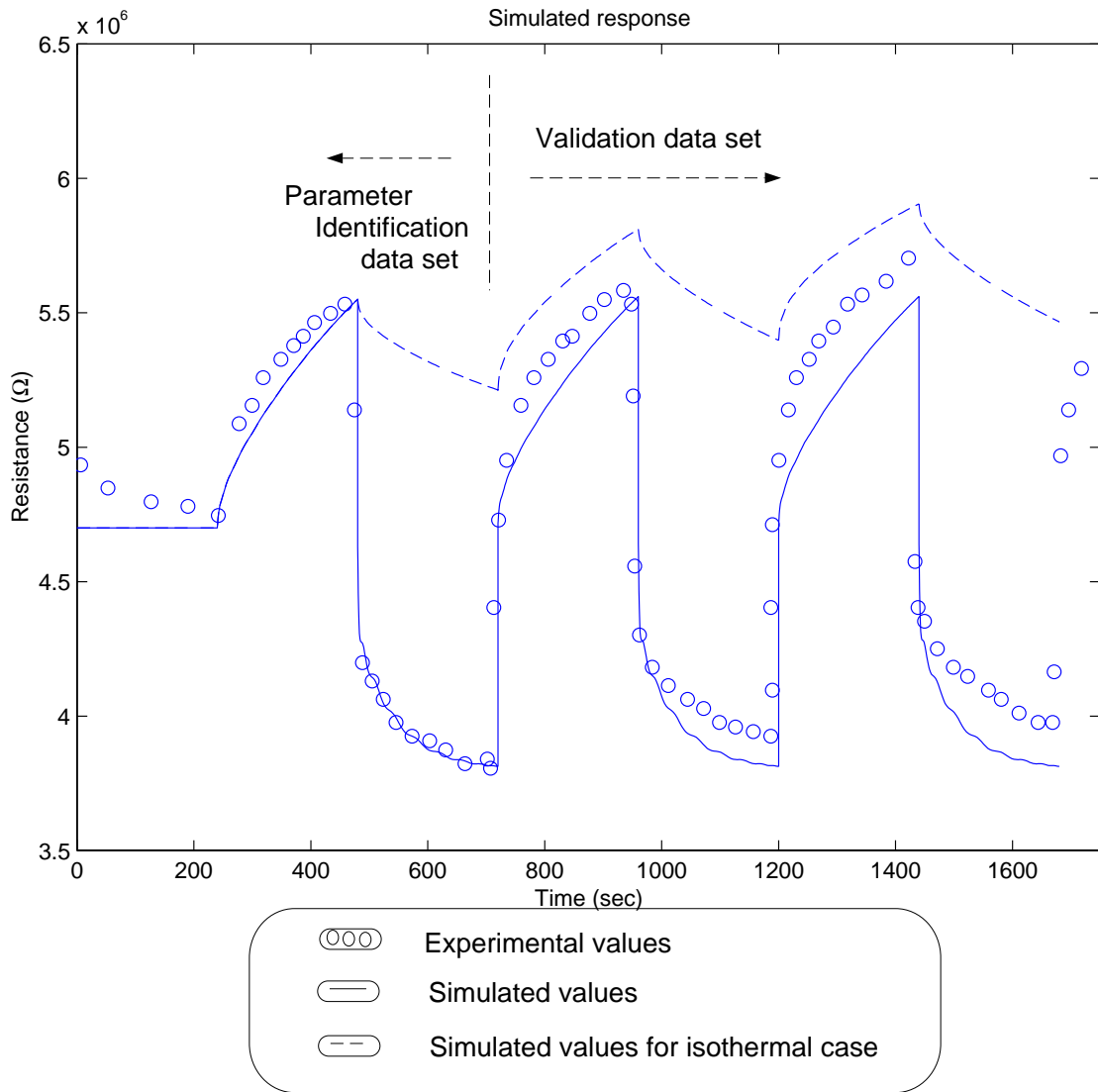
Figure 4.7: Comparison of experimental and simulated resistance profiles of micro-hotplate based sensor for NH_3 gas using twenty collocation points in time.

There is a good match between the resistance values obtained experimentally and those calculated by simulation. The experimental resistance values increase in the subsequent cycles. The model predicts an ideal case where the gas is driven out completely, hence the base resistance does not drift. However, in practice, gases are not driven off completely. The gas can undergo irreversible reaction with the π bonds and cause permanent degradation of the polymer. This is in accordance with the theory of stability of the conducting polymer. The dashed curve indicates the drift in the resistance in case of absence of heating. The difference would further increase in the subsequent cycles. The change in the resistance value and sensitivity decreases if the desorption is carried out at ambient temperature.

Chapter 5

Conclusions and Future Work

5.1   Concluding remarks

The electrical response of the sensor, based on a design of NIST researchers [27], to the variations in the gas concentration is modeled. The model is based on partial differential equation-based models of the species diffusion through the polymer film, coupled with sorption kinetics expressions. The time-dependent, nonlinear boundary-value problems is solved using global spectral methods software. The PDE's were solved using 40 quadrature points along the length of the polymer film and six collocation points in time. 16 eigenfunctions were computed using a Sturm-Liouville solver.

The diffusion rate of gaseous species in the polymer, rate of adsorption and desorption of the gaseous species on the vacant sites and gas sensitivity coefficient of the polymer are estimated using *lsqnonlin* function of the *MATLAB* optimization toolbox. The simulated results based on the estimated parameters match the experimental values over a sequence of six adsorption and desorption cycles for the oxidizing (NO_x) and reducing (NH_3) gas species measured by Kendrick and co-workers [27].

In cases where the sensor is operated at ambient temperature, the gaseous species do not desorb completely even if the sensor is not exposed to gaseous species for a long period of time. This leads to a drift in the base resistance and reduced sensitivity. However simulations indicate at elevated temperature the gaseous species desorb rapidly. The comparison of the parameters at ambient and elevated temperature show that the rate of diffusion increases by an order of magnitude. The rate of the desorption reaction increases by a factor of 38.5 and is twice the rate of the adsorption reaction at elevated temperature. Hence variation of temperature serves as an efficient sensor cleaning technique. The base resistance of the sensor and the sensitivity remains almost constant over multiple cycles.

The simulation results indicate the rate of adsorption and desorption of gases. This information can be used to tune the adsorption/desorption cycle time of the sensor. For example, the desorption takes place rapidly at elevated temperature, hence the desorption cycle time can be reduced. This would improve the overall response of the sensor. If the rate of adsorption of gases through the polymer film is slow, adsorption cycle time might have to be increased to improve the sensitivity of the sensor. Hence the simulation result can be used to optimize the cycle time of the micro-sensor.

5.2 Future Work

5.2.1 Multicomponent systems

In the case of gas mixtures, each individual gas affects the conductivity of the polymer film. The change in resistance is the only sensor output available. So

it may be difficult to analyze the response of each gas. Improving the selectivity and sensitivity of the conducting polymer to a desired gas can solve the problem.

Selection of the monomer, which has greater affinity for the chemical to be tested, can improve the selectivity of the sensor. The dopant level affects the base conductivity. Hence, percentage of the dopant in the conducting polymer can be varied to improve sensitivity of the sensor. A multidimensional array of conducting polymers having different characteristics can be used along with pattern recognition technique for detection of multiple gases.

The sensor can be operated in a dynamic mode in which the temperature is varied during the operation. Temperature dependence of diffusion of gas in the polymer film and rate of adsorption and desorption differs among the gas species. Hence the desired gas species can be selectively adsorbed or desorbed by varying the temperature.

5.2.2 Frequency based interrogation techniques

The measurement of multiple electrical parameters namely resistance, capacitance and dissipation factor as a function of frequency, enables a multi-parametric technique for identification of chemical species. The AC resistance response of the sensor is 24% at 1MHz. as compared to DC response of 4%. The capacitive response is highest at 31% and 34% at 600 and 700MHz respectively [3]. Hence the additional frequency parameters make the sensor normally relatively unselective at DC more selective when exposed to volatile chemicals such as methanol, acetone and ethyl acetate [5].

The dissipation factor is an indicator of the change in dipole-dipole interaction occurring when a volatile chemical becomes adsorbed on the polymer film. Dissi-

pation factor is the ratio of resistance and reactance. At the resonant frequency the reactive part of the impedance approaches zero and hence the dissipation factor becomes very high. The position of the peak in the frequency domain depends on the chemical and the height of the peak depends on the concentration of the gas. In case of mixture of gases, multiple peaks are obtained on one to one correspondence with the gas species [4].

FT-sensor

The frequency-based sensors are continuous wave (CW) instruments. In the CW operational mode, the frequency of the electric field is varied. The electrical parameters are recorded at each frequency. After the frequency is increased, the measurement can be made only after the system stabilizes. Additionally the difference between consecutive frequency measurements should be small to obtain a fine resolution. Hence overall the response of the sensor is very slow and cannot be used for online measurement.

In the pulse technique a single rectangular pulse modulated at monochromatic RF serves as electrical input to the sensor. The output signal of the sensor is measured after the pulse is turned off. The record of the receiver voltage in the time domain is called the free induction decay (FID). Fourier transformation is required to transform the resulting signal from the time domain to frequency domain to obtain a useful form. An example of electrical output of the sensor in the time domain (FID) is given in figure (5.2). The FID is converted from time domain to frequency domain using Fast Fourier Transform (figure 5.3). The steps involved in the FT-sensor are outlined in figure (5.1).

A rectangular pulse modulated at monochromatic RF f_s can be described in

RF pulse

Electrical input

Sensor

Electrical Output

Free Induction decay

Fast fourier transform

Frequency response
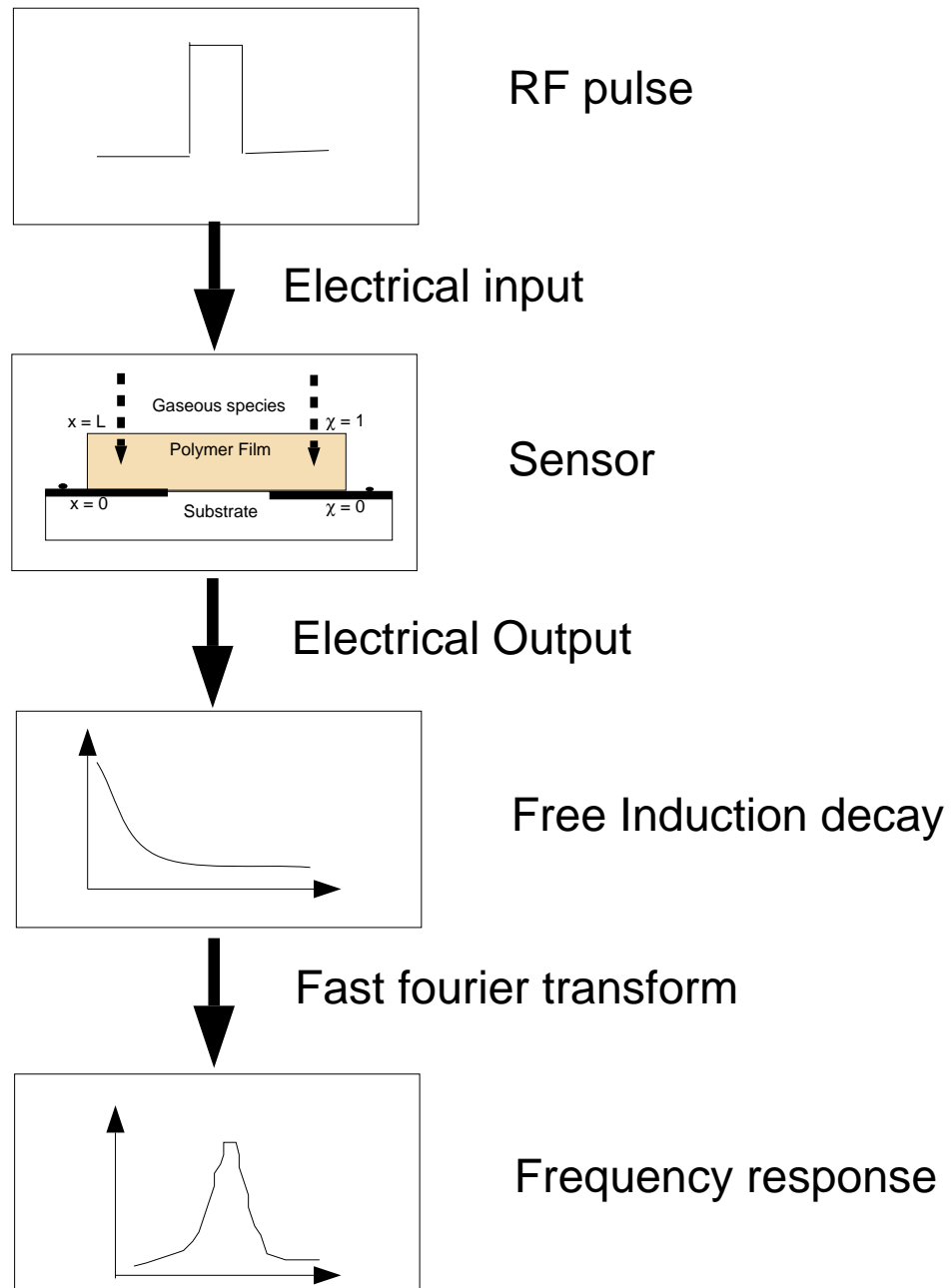
Figure 5.1: FT-sensor
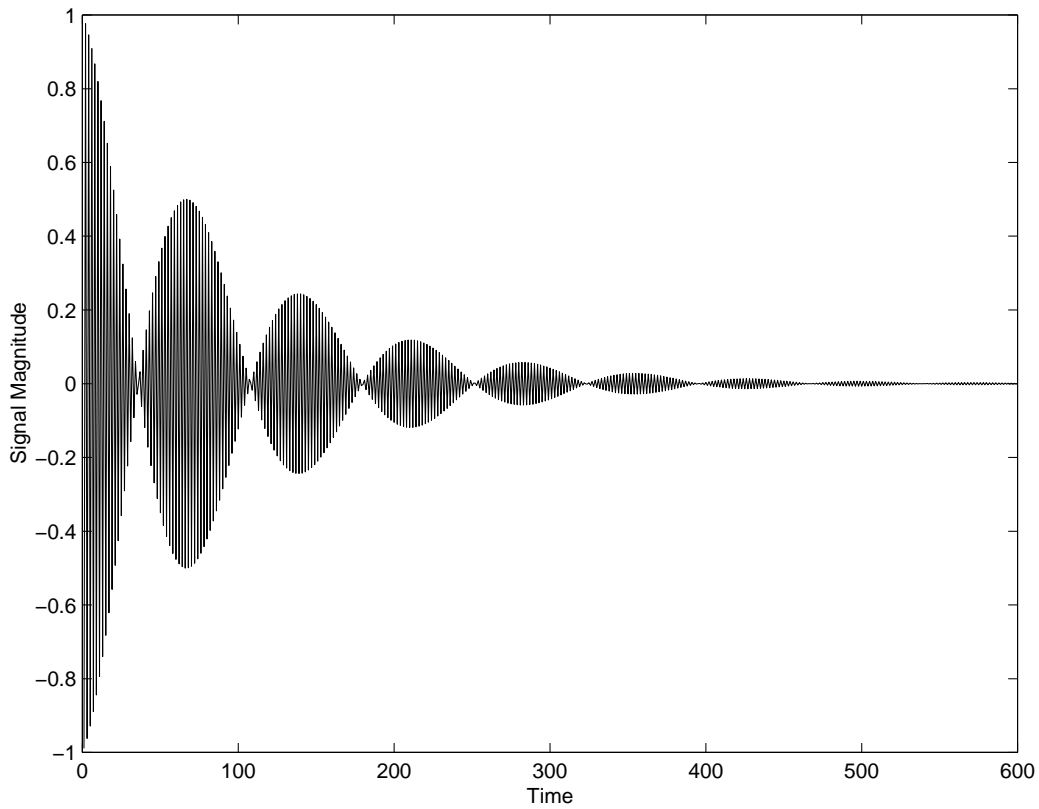
Figure 5.2: Electrical output of the sensor in the time domain (FID).
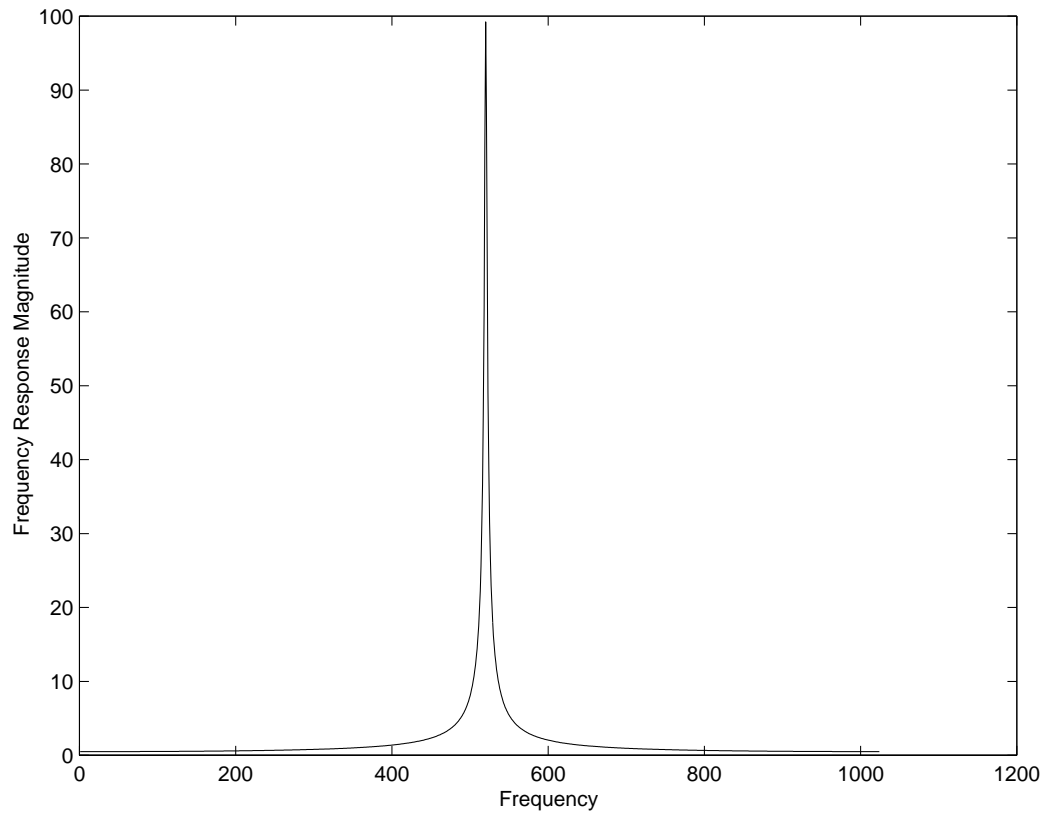
Figure 5.3: Electrical output of the sensor converted to frequency domain.

the frequency domain as a band of frequency centered at the RF frequency . The frequency domain response of a rectangular RF pulse of width t_p and frequency f_s and amplitude A is given by equation (5.1).

$$A\left(Sinc\left(\frac{\pi(f - f_s)}{t_p}\right)\right) \tag{5.1}$$

The frequency band depends on the pulse width. As the width decreases frequency band increases. A shorter pulse results in a lower power at the center as the energy is spread over a wider frequency band. Hence the RF generator should be capable of delivering a short and high-powered pulse. The frequency domain signals for square pulses of width 10 seconds and 100 seconds and modulated at 1 kHz are plotted in figures (5.4) and (5.5) respectively.

5.2.3   Gas sample preconcentrator

Preconcentrator system can improve the sensitivity and selectivity of the microsensors. Preconcentrator would increase the concentration of the gas species and also separate the desired gas species from the mixture. The schematic diagram of the preconcentrator is given in figure (5.6). Preconcentrator consists of an adsorbent material embedded in a metal cylinder with open top and bottom surface. The curved metallic surface is heated using electrical heater. The temperature on the surface is controlled using microprocessor based temperature controller. There is an arrangement to control the flow of gas in the preconcentrator.

Initially the adsorbent is maintained at ambient temperature. The top of the adsorbent material is exposed to gas. The gas diffuses through the adsorbent material and gets adsorbed on the surface of the adsorbent. The temperature of the surface is then increased to a predetermined temperature and the flow of gas in the preconcentrator is stopped. The gas desorbs and leaves the preconcentrator
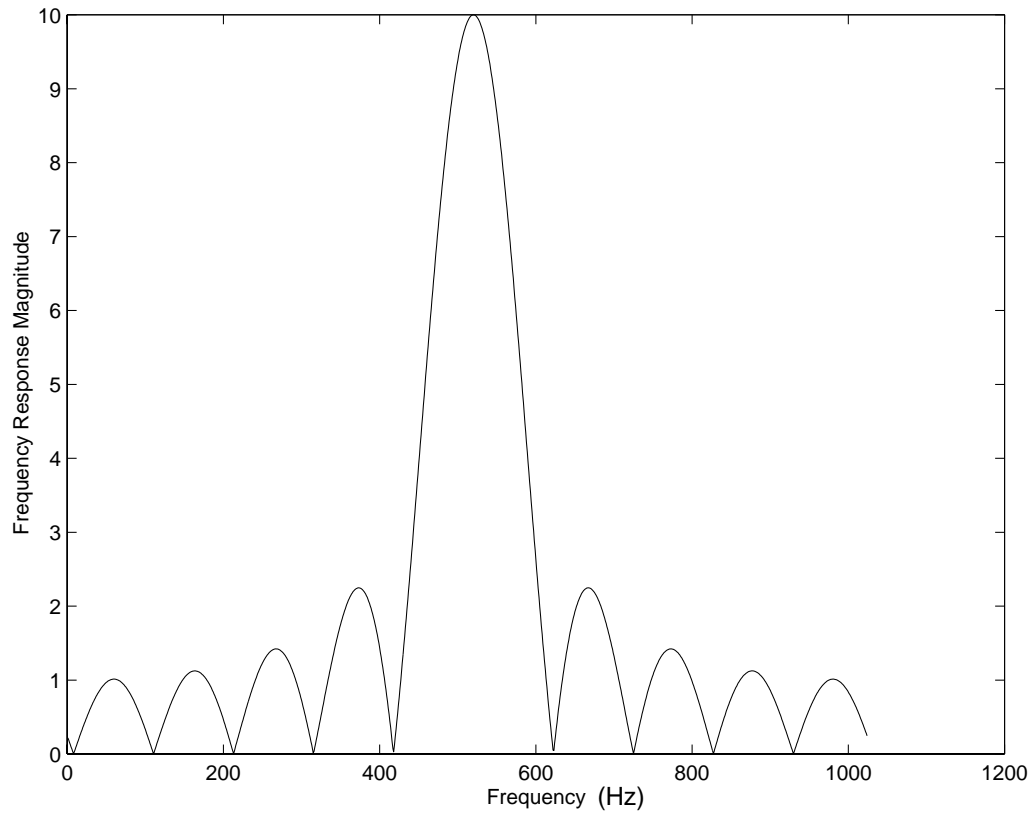
Figure 5.4: Frequency domain representation of a square pulse of width 10 milli seconds modulated at frequency 1 kHz.
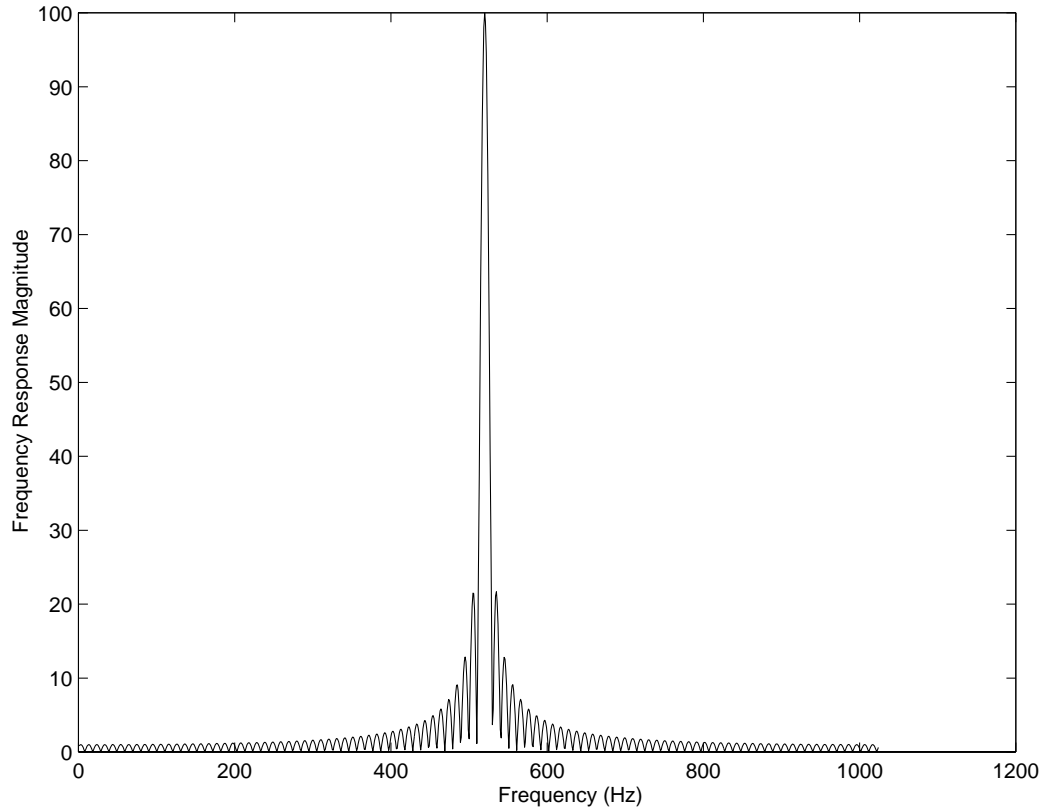
Figure 5.5: Frequency domain representation of a square pulse of width 100 milli seconds modulated at frequency 1 kHz.
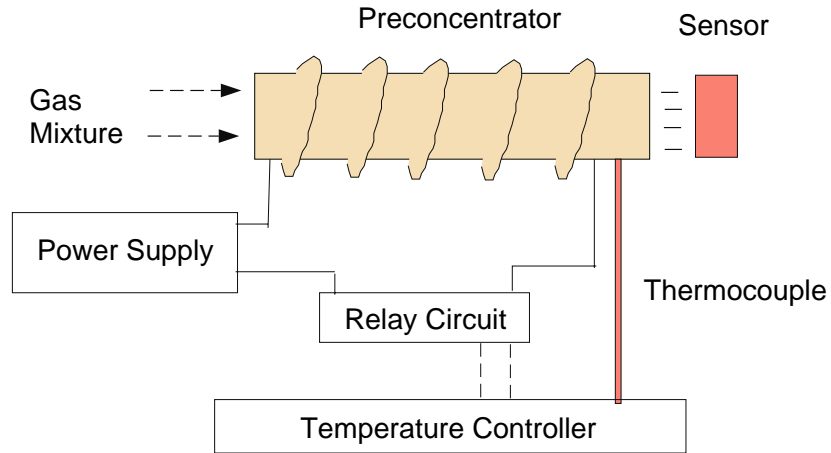
Figure 5.6: Preconcentrator

from the bottom of the preconcentrator. The concentrated gas species serves as input to the sensor. This improves the sensitivity of the sensor.

The selectivity of the sensor can be improved by selective thermal desorption of gas from the preconcentrator. The temperature of the preconcentrator is raised to a temperature where the desired gas species desorbs faster than the remaining gas species. Adsorbent that selectively enables faster adsorption of the desired gas species also improves selectivity of the micro-sensor.

BIBLIOGRAPHY

[1] Adomaitis, R. A. and Lin, Y. -h., A collocation/quadrature-based Sturm-Liouville solver, *Appl. Math. Comp.*, Vol. 110, 205 - 23 (2000).

[2] Adomaitis, R. A., Y. -h. Lin, and H. -Y. Chang, A Computational Framework for Boundary-Value Problem Based Simulations, *Simulation*, Vol. 74, 28 - 38 (2000).

[3] Amrani, M. E. et. al., High Frequency measurement of organic conductivity polymers : development of a new technique for sensing volatile chemicals, *Meas. Sci. Technol.*, Vol. 6(5), 1500 - 7 (1995).

[4] Amrani, M. E. et. al., Mutlifrequency measurement of organic conductivity polymers for sensing of gases and vapours, *Sensor and Actuators B.*, Vol. 33, 137 - 41 (1996).

[5] Amrani, M. E. et. al., Synthesis Characterisation and multifrequency measurement of poly-N-(2pyridyl) pyrrole for sensing volatile chemicals, *Material Science Eng. C*, Vol. 1, 17 - 22 (1993).

[6] Alcacer L. (ed.), *Conducting polymers ; special applications : proceedings of the workshop held at Sintra, Portugal* Boston : Kluwer Academic Publishers, c1987.

[7] Benseddik, E., Makhlouki, M., Bernede, J. C., Lefrant, S., Pron, A., XPS studies of environmental stability of polypyrrole-poly(vinyl alcohol) compos-

ites, *Synthetic Metals*, Vol. 72(3), 237 - 42 (1995).

[8] Brie, M., Turcu, R., and Mihut, A., Stability study of conducting polypyrrole films and polyvinylchloride-polypyrrole composites doped with different counterions, *Materials Chemistry and Physics*, Vol. 49(2), 174 - 8 (1997).

[9] Bianco, B., Parodi, M., and Degani, G., A circuit Theorectic approach for deriving the electrical properties of statistical properties, *Alta Frequenza* , Vol. 51, 80 - 85 (1982).

[10] Bianco, B., and Bonfiglio, A., An electrical model for two-dimensional layers of conductive polymers, *Thin solid films*, Vol. 284 - 285, 520 - 2 (1996).

[11] Blackwood, D., Josowicz, M., Work function and spectroscopic studies of interaction between conducting polymers and organic vapors, *J. Phy. Chem.*, Vol. 95, 493 - 502 (1991).

[12] Britz, D., *Digital Simulation in Electrochemistry*, New York : Springer-Verlag, c1981.

[13] Child, A. D., Kuhn, H. H., Enhancement of the thermal stability of chemically synthesized polypyrrole, *Synthetic Metals*, Vol. 84(1-3), 141 - 2 (1997).

[14] Chen, X.B., Issi, J.-P., Devaux, J., Billaud, D., The stability of polypyrrole and its composites, *Journal of Materials Science*, Vol. 32(6), 1515 - 8 (1997).

[15] Dai, E., et. al., Organic Vapor Sensors based on SAW resonators and organic film *IEEE Transactions on Ultrasonics, Ferroelectrics and frequency control*, Vol. 44(2), 309 - 13 (1997).

[16] Gardner, J. W., Modeling of gas-sensitive conducting polymer devices, *IEEE Proc. - Circuits Devices Syst.*, Vol. 142(5), 321332 (1995).

[17] Gardner, J. W., Diffusion and binding of molecules to sites within homogenous thin film, *Tran. Roy. Soc.*, (1995).

[18] Gardner, J. W.(ed.), and Bartlett P. N.(ed.), *Sensors and Sensory Systems for an Electronic Nose*, Boston : Kluwer Academic Press, c1992.

[19] Gardner, J. W., Electrical conduction in solid-state gas sensors *Sensors and Actuators*, Vol. 18, 373 - 87 (1989).

[20] Gottlieb D., Orszag S. A., *Numerical analysis of spectral methods : theory and applications*, Philadelphia : Society for Industrial and Applied Mathematics, c1993.

[21] Grate, J. W., Rose-Pehrssson, S. L., Venezky, D.L., Klusty, M., and Wohltjen, H., Odor sensing system using preconcentrator with variable temperature, *Anal. Chem.*, Vol. 65, 1868 - 70 (1993).

[22] Hwang, B. J., et. al., A microscopic gas-sensing model for ethanol sensors based on Conductive polymer composite from polypyrrole and poly(ethylene oxide), *J. Electrochemical Society*, Vol. 146(3), 1231 - 36 (1999).

[23] Huang J., An object oriented programming approach to implement global spectral methods : application to dynamic simulation of a chemical vapor infiltration process, *Master's Thesis* (2000).

[24] Janata J., *Principles of Chemical sensors* , New York : Plenum Press, c1989.

[25] Josowicz, M., and Topart, P., Studies of the interactions between organic vapours and organic semiconductor applications to chemical sensing' in Gardner, J. W. and Bartlett P. N., *Sensors and Sensory Systems for an Electronic Nose* , Boston : Kluwer Academic Press, 117-129, c1992.

[26] Kemp, N. T., et. al., Thermoelectric Power and conductivity of different types of polypyrrole, *J. Polymer Science : Part B: Polymer Physics*, Vol. 37, 953 - 60 (1999).

[27] Kendrick C., Cavicchi R.E. and Semanick S., Improved performance of polymer microsensor using fast thermal conditioning, *to be published*.

[28] Kunt, T., McAvoy T.J., Cavicchi R. and Semanick,S., Dynamic modeling and optimization of microhotplate chemical gas sensors,*IFAC, AD-CHEM'97*(1997).

[29] Lin, C.W., Hwang, B.J., and Lee, C.R., Methanol sensors based on the conductive polymer composites from polypyrrole and poly(vinyl alcohol), *Materials Chemistry and Physics*, Vol. 55(2), 139 - 44 (1998).

[30] Lin, Y. -h., Chang, H. -Y., and R. A. Adomaitis 1999, MWRtools: A library for weighted residual methods. *Comp. & Chem. Eng.*, Vol. 23, 1041 - 61.

[31] *Matlab Reference Guide*, The MatlabWorks,Inc., c1992.

[32] Milella, E. et. al., Polypyrrole LB multi-layer sensitive films for odorants, *Thin Solid Films*, Vol. 284-285, 908 - 10 (1996).

[33] Omastova, M., Kosina, S., Pionteck, J., Janke, A., and Pavlinec, J., Electrical properties and stability of polypyrrole containing conducting polymer composites, *Synthetic Metals*, Vol. 81(1), 49 - 57 (1996).

[34] Payne, P. A., et. al., Gas Sensors, *UK Patent*, GB2 203 553B (1990).

[35] Skotheim T. A. (ed.), *Handbook of conducting polymers*, New York : M. Dekker, c1986.

[36] Slater, J.M., Watt, E.J., Freeman, N.J., May, I.P. and Weir, D., Gas and vapor detection with polypyrrole sensors, *Analyst*, Vol. 117, 1265 - 70 (1992).

[37] Semanick,S. and Cavicchi R.,Kinetically controlled chemical sensing using micromachined structure, *Accounts of Chemical Research*, Vol. 31(5), 279 - 87 (1998).

[38] Topart, P. and Josowicz, M., Characteristic of the interaction between polypyrrole films and methanol vapours, *J. Phys. Chem.*, Vol. 96, 7824 - 30 (1992).

[39] Truong, V.-T., Ennis, B.C., and Forsyth, M., Ion exchange, anisotropic structure and thermal stability of polypyrrole films, *Synthetic Metals* , Vol. 69(1-3), 479 - 80 (1995).

[40] Vieth W. R., *Diffusion in and through polymers : principles and applications*, New York : Oxford University Press, c1991.

[41] Isaka, Y., Nakamoto, T., Moriizumi, T., and Grate, J. W., Odor sensing system using preconcentrator with variable temperature, *Sensors and Actuators B* , Vol. B69(1-2), 58 - 62 (2000).

[42] Yueqiang, S., and Carneiro, K., Characteristion of the transport properties of conducting polypyrrole films, *Synthetic metals* Vol. 18, 77 - 83 (1987).

[43] Zee, F., and Judy, J., MEMS chemical gas sensor, *Proceedings of the Thirteenth Biennial University/Government/Industry Microelectronics Symposium* , New Jersey : IEEE Piscatatway, 150 - 2.